https://doi.org/10.1016/j.ijhydene.2017.10.004

Modelling the triple phase boundary length in infiltrated SOFC electrodes

1. Periasamy Vijay[a,*]

Email: V.Periasamy@curtin.edu.au

Ph: +61 8 9266 9890

2. Moses O. Tadé[a]

Email: V.Periasamy@curtin.edu.au

Ph: +61 8 9266 4800

3. Zongping Shao[a]

Email: zongping.shao@curtin.edu.au

Ph: +61 8 9266 4702

4. Meng Ni[b]

Email: meng.ni@polyu.edu.hk

[a]Centre for Process Systems Computations, Department of Chemical Engineering, Curtin University, Western Australia 6845, Australia

[b]Building Energy Research Group, Department of Building and Real Estate, The Hong Kong Polytechnic University, Hung Hom, Kowloon, Hong Kong, China

*Corresponding author

Modelling the triple phase boundary length in infiltrated SOFC electrodes

Periasamy Vijay[a], Moses O. Tadé[a], Zongping Shao[a], Meng Ni[b]

[a]Centre for Process Systems Computations, Department of Chemical Engineering, Curtin University, Western Australia 6845, Australia

[b]Building Energy Research Group, Department of Building and Real Estate, The Hong Kong Polytechnic University, Hung Hom, Kowloon, Hong Kong, China

Abstract

A model based on the principles of coordination number and percolation theory is proposed for calculating the triple phase boundary (TPB) lengths in the Solid Oxide Fuel Cell (SOFC) electrodes infiltrated with nano particles. The TPB length is a critical microstructural property that influences the cell performance. Empirical expressions for the overall average coordination number and percolation probabilities are proposed to compliment the basic model framework provided by the coordination number principles. The comparison with the numerical and analytical model results from literature is used to both evaluate and interpret the proposed model. The model demonstrates reasonable agreement with literature model and experimental results and provides insights into the coordination number behaviour. This model is a potential alternative to the expensive numerical simulations for the microstructural optimisation of the infiltrated electrodes.

Keywords: SOFC; Infiltrated electrodes; Modelling; Triple phase boundary

1. Introduction

Infiltration of electrodes with nanoparticles is a very effective method to improve the performance of Solid Oxide Fuel Cells (SOFCs). Apart from increasing the total triple phase boundary (TPB) length, infiltration also results in creating better contact between the electrode and the electrolyte and can potentially minimise the thermal expansion mismatch between these two layers [1]. As there is a window of volumetric percentages of the electronic and ionic conducting particles in the SOFC electrodes that can offer decent performances, there is scope for design and optimisation of the electrodes with respect to the particle composition, sizes and electrode porosity. The design and optimisation tasks will be greatly simplified if supplemented by mathematical models.

Several models for the conventional composite electrodes have been proposed in the literature. A purely geometric model for the TPB length is proposed in [2]. In the work of [3], the electrode particles are treated as perfect spheres and the principles of coordination numbers and the percolation theory are used to formulate the microstructural model defining the triple phase boundary lengths. This micro structural model is then used in the framework of the macro-model to predict the cell performance. In reference [4], similar principles were used to create a model for calculating the TPB length in SOFC electrodes. The coordination number principles employed in these works were largely based on the work on binary powder mixtures in [5]. Reference [6] provided an alternate formulation that satisfies the contact number conservation principles and is based on the theory provided in [7].

One of the methods to obtain the electrode properties like the TPB length is through the reconstruction the 3D microstructure of the infiltrated electrodes. A successful method used in the case of conventional composite electrodes is the 3D microstructure reconstruction using imaging techniques such as FIB-SEM. However, this method faces resolution problems with the nanoparticles in the case of infiltrated electrodes [8]. Another method consists of numerically simulating the deposition process to construct the electrodes from which the effective properties are calculated [1, 8-10]. The successful implementation of this method results in the identification of the TPB lengths for a wide range of microstructural parameters. A comprehensive work on the microstructural properties of the infiltrated electrodes of the SOFC are studied through numerical simulations in [8]. Although the numerical methods are more reliable, it is difficult to integrate this method with higher level macroscopic model for multi-scale simulations. Thus, there is a need to develop simpler yet sufficiently accurate models to construct the microstructure of the infiltrated electrodes.

Compared to the conventional electrodes, relatively less effort has gone into the modelling of infiltrated electrodes. A geometric treatment of the impregnated electrode is provided in reference [11]. The derivation assumes a uniform single layer coating of nano particles over the backbone substrate. As a result, this formulation cannot consider variations in the particle compositions and hence has limited application in designing electrodes. An analytical model for the TPB length was proposed in [8]. The model features the unoccupied area of the backbone particle as the independent variable, which itself is calculated by solving differential equations with three fitting parameters. In [1, 12], percolation theory

and geometric arguments are used to obtain a model for the TPB length of infiltrated electrode. The experimental relations between conductivity and the nano particle volume fraction are used to derive the site occupation probability, from which the percolation probability and the effective TPB are obtained. In the work of [13], the TPB length was defined in terms of the coordination numbers akin to the treatment in the works on the conventional electrodes. But, the coordination numbers were themselves derived from numerical simulations. In our work, we present an analytical model for the TPB of the infiltrated electrodes which is purely based on the percolation theory and coordination number principles. This is achieved using an empirical expression for the overall coordination number of the infiltrated electrodes. In addition to predicting the TPB length, this model also provides insights into the particles contact behaviour in infiltrated electrodes. Correlations for the pore and infiltrated particle percolation probabilities are also presented. The presented model can be useful for the microstructural optimisation of the infiltrated electrodes. It can also be easily integrated with higher level macroscopic models for multi-scale simulations.

2. Triple phase boundary length model for the infiltrated electrodes

The model proposed for the infiltrated electrodes TPB area calculation is based on the concepts of coordination numbers and percolation theory that have been previously used in the modelling of the conventional composite SOFC electrodes [6] [3]. A schematic of the electrode with its backbone framework infiltrated with nano particles is shown in Fig. 1. Infiltration is generally achieved by precipitating a metal salt solution into a porous backbone structure followed by the decomposition of the metal salt [14].

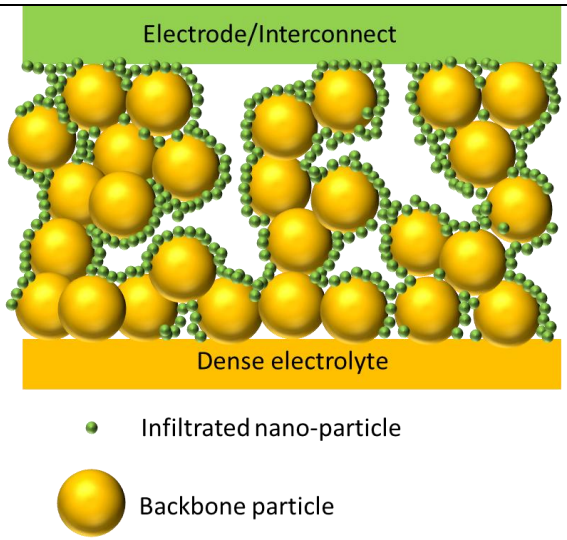

Fig. 1: Schematic of the infiltrated electrode

The following relations result from the concept of coordination numbers that enumerate the average number of contacts between particles touching each other [5] [7]. For our application, there are two kinds of particles, namely the micro sized backbone particles and the nano-sized infiltrated particles. The average coordination numbers with respect to each particle are defined as Z_B and Z_n. Z_B represents the average number of all particles (both backbone and the nano particles) that are in contact with the backbone particle and Z_n is similarly defined. Z_B and Z_n can themselves be broken down into two components each as described in the following relations.

$$Z_B = Z_{B,B} + Z_{B,n} \tag{1}$$

$$Z_n = Z_{n,n} + Z_{n,B} \tag{2}$$

Where $Z_{x,y}$ is defined as the average number of *y* particles in contact with an *x* particle. Using the number fractions of these two types of particles, an overall average coordination number for the two particle system can be defined as follows.

$$Z = \zeta_B Z_B + \zeta_n Z_n \tag{3}$$

The contact number conservation principle provides another relation between $Z_{n,B}$ and $Z_{B,n}$.

$$\zeta_B Z_{B,n} = \zeta_n Z_{n,B} \tag{4}$$

Using the relations in Eqs. 1-4, we can obtain the following expressions for $Z_{n,B}$ and $Z_{B,n}$.

$$Z_{n,B} = \frac{Z - Z\zeta_n S_n - Z_{B,B}\zeta_B}{2\zeta_n} \tag{5}$$

$$Z_{B,n} = Z_{n,B}\frac{\zeta_n}{\zeta_B} \tag{6}$$

For a given particle composition in a conventional electrode, both the electronic and ionic conducting particles are randomly arranged in such a manner that the overall average coordination number remains constant. However, in the case of the infiltrated electrodes, the backbone structure is initially formed with fixed coordination number, into which, the nano particles are impregnated.

Given the backbone structure porosity (ϕ_B) of the electrode, the number of backbone particles per unit volume can be approximated by the following expression [1].

$$n_B = \frac{3(1-\phi_B)}{4\pi r_B^3} \tag{7}$$

The number of nano-particles per unit volume depends on the nano-particle volume fraction as follows.

$$n_n = \frac{\zeta_n}{\zeta_B} n_n$$

(8)

The porosity of the electrode changes as the nano particles are infiltrated into the pore space. This porosity can be given in terms of the initial backbone structure porosity as follows:

$$\phi = \phi_B - \frac{4n_n\pi r_n^3}{3} \tag{9}$$

The average coordination number $Z_{B,B}$ corresponding to the backbone particles can be reasonably assumed to be equal to 6, since the random packing of spherical particles with a single radius results in this average coordination number based on simulation and experimental evidence [5]. This assumption is also used in other works for single particle case [11] [12] and for binary particle packing [3, 6]. In fact, this assumption is also true for

two particle case where the particles have different sizes. However, it must be noted that the process in which the particle arrangement happens in infiltrated electrodes is different from the conventional electrodes. In the former, the backbone particle is initially formed with a porous structure and then the nano-sized infiltrations are deposited, while in the latter both type particles are mixed together before being processed to produce the final porous structure. Therefore, while it is reasonable to assume that the overall coordination number is six in the conventional electrodes, this is not true for the infiltrated electrodes. Moreover, a fixed overall average coordination number (*Z*) is unable to reproduce the peaking phenomena of the TPB length observed in the literature evidences. While the fixed *Z* works for the conventional composite electrode case, it doesn't in the case the infiltrated electrodes primarily due to the different definition of the particles numbers as provided in Eq. 7 and 8.

We hypothesise that the overall coordination number of the infiltrated electrode keeps changing as the infiltration loading is increased. The overall coordination number depends on both the surface area fraction of the backbone particles and the infiltration particles. The effect of agglomeration tends to increase the effect of the surface area of the backbone particles (more nano particles tend to settle on other nano particles leaving more back bone particle surface free) and decrease the effect of the surface area of the infiltrated particles (more nano particles have the affinity to settle on the backbone particle). Considering these, the following empirical expression for the overall average coordination number is proposed.

$$Z = \alpha S_B^{w} S_n^{1-w}, \tag{10}$$

where w accounts for the agglomeration effect of the infiltrated particles. The value of w varies between 0 to 1. Low values of w indicates high agglomeration risk and vice versa. Low values of w will give more weightage to the backbone particle surface fraction whereas high w values will give more weightage to the nano particle surface area. The agglomeration phenomena can result in influencing the magnitude of the peak TPB length and the electrode composition corresponding to the peak TPB length as can be observed from the numerical results from [8]. The power terms for the surface area fractions in the expression for Z account for the shift in the TPB length peaks associated with the agglomeration effect. To account for the effect of the agglomeration phenomena on the peak TPB magnitudes,

the α term is formulated as a function of w and the following logarithmic function offers the best agreement with the available numerical results.

$$\alpha = a_1 \ln w + a_2$$

(11)

Where $a_1 = 4.0839$ and $a_2 = 16.388$.

The component $Z_{n,n}$ is defined in the manner similar to the conventional electrodes as given in Eq. 12 [7] [15]. It is rational to consider that $Z_{n,n}$ depends on the surface area fraction S_n. Considering that the overall average coordination number Z is not constant, $Z_{n,n}$ will also depend on the agglomeration effects.

$$Z_{n,n} = ZS_n \tag{12}$$

Taking into account that the contact angle of the nano particles with the backbone particles is 90^o [8], the total triple phase boundary length per unit volume is given as the following.

$$\lambda_{tot} = 2\pi r_n n_n Z_{n,B} \tag{13}$$

The active triple phase boundary length per unit volume can be defined using the infiltrated particles percolation probability and the pore percolation probability as:

$$\lambda_{act} = 2\pi r_n n_n Z_{n,B} P_n P_p \tag{14}$$

The percolation of the backbone particle is not considered here similar to [8]; the reason being that the backbone is formed prior to the infiltration and therefore will be fully percolated.

One of the important analysis that can be performed with the micromodels of the electrodes is the variation of properties like the TPB length with different compositions of the electronic and ionic conduction materials [3, 6] [1, 10, 12, 16]. This analysis can help us in determining the ideal composition that maximises the TPB length. In the case of the conventional composite electrodes, the electrode porosity is independently determined and the analysis is carried out by increasing one type of particle content (say electronic). This increase in electronic particle content must be accompanied by decreasing the ionic particle content so as to maintain the porosity. However, in the case of infiltrated electrodes [16] [8], the analysis usually considers a fixed backbone structure porosity (and fixed backbone

particle volume fraction) and the increase in infiltration loading leads to decreasing porosity of the electrode.

Since the electrode porosity rather than the backbone porosity is a key design variable, we also study the case with fixed electrode porosity but variable backbone porosity. In this case, the number of backbone particles will also change in addition to the infiltrated nano particles as the infiltration loading is varied. The number of backbone particles and the number of nano-particles per unit volume for this case are given as follows.

$$n_B = \frac{3(1-\phi)\psi_B}{4\pi r_B^3} \tag{15}$$

$$n_n = \frac{3(1-\phi)\psi_n}{4\pi r_n^3}$$

(16)

where ϕ is the desired electrode porosity.

2.1. Percolation probabilities:

Expressions for the pore and the infiltration percolation probabilities are required for calculating the TPB length in Eq. 14. In previous modelling studies for the conventional composite SOFC electrodes [3, 5, 6], the percolation probabilities for electronic (P_{el}) and ionic conducting particles (P_{io}) were formulated as empirical relations. The relation for P_{el} was given in terms of the coordination number component $Z_{el,el}$ and the relation for P_{io} was provided as a function of $Z_{io,io}$. These relations were developed based on experimental and simulation data.

Unlike the conventional composite electrode case, $Z_{n,n}$ is not suitable for formulating a relation for the nano-particle percolation owing to its change in direction around the critical values of the infiltration loading. Therefore, several variables were studied for their suitability to form empirical relations to represent the infiltration particle and pore percolation probabilities. The nano particle surface area fraction is a good variable for defining the infiltrated particle percolation. This conclusion is arrived based on the dependencies of the percolation probability on the geometric and other microstructural parameters as reported in [8]. It is observed that the infiltrated particle percolation is sensitive to the backbone particle diameter with the decreasing diameter increasing the

percolation threshold with respect to the infiltration loading. This behaviour can be understood considering that for a given volume fraction, smaller the backbone particle diameter, more will be the number of particles, which will make the porous structure more difficult to penetrate. This results in requiring a larger infiltration loading to achieve percolation. The opposite effect is observed with the nano particle diameter. In this case, larger diameter results in larger percolation threshold as the difficulty for forming a uniform layer increases. The porosity of the backbone structure also has an effect on the infiltration percolation threshold which is similar to the backbone particle size effect. More the starting porosity, more early will the percolation threshold occur due to the relative easiness for the nano particles to form a continuous layer on the backbone surface. Finally, lesser the agglomeration, more early is the infiltration percolation threshold obtained due to the ease of uniform deposition.

The surface area fraction of the nano particles (S_n) is a suitable variable for the purpose of formulating a relation for the nano particle percolation probability (P_n). The nano particle surface area fraction will decrease with the increase in the backbone particle size. This implies that the same surface area fraction will be reached at a lesser infiltration loading for a larger backbone particle size compared to a smaller size. The exact opposite effect will be achieved with the changing nano particle size. The surface area fraction will also be sensitive to the starting backbone particle structure's porosity. More porosity results in higher nano particle surface area fraction due to the decrease in backbone surface area and vice versa. However, the agglomeration tendency will not have any effect on the nano particle surface area fraction. All these can be verified from the plots in Fig. 2. The Fig. 2a shows the behaviour of the nano particle surface area fraction for varying back bone particle sizes throughout the infiltration loading range. The Fig. 2b shows the variation of the surface area fraction with the backbone porosity and Fig. 2c shows its variation with nano particle size. The Fig. 2d shows the variation of the surface area fraction with different values of w. All the three curves in the figure are superimposed suggesting that w has negligible influence on the surface area fraction. From these, it can be understood that the infiltrated particle surface area fraction has a behaviour that reflects the behaviour of the percolation probability except for the case of varying w. For the lack of other suitable variables, we

choose the nano particle surface area to formulate the relation for the infiltrated particle percolation probability.

In Fig. 3, the infiltrated particle percolation probability from the numerical simulations in [8] is plotted against the nano particle surface area fraction. The data are presented for several conditions with varying particle radii, porosity and 'w' as available in [8]. The S_n values computed by the model for a given infiltration loading are plotted against the percolation probability for the same loading. It can be seen that the transition of the probability from 0 starts roughly between S_n values of 0.45 and 0.6 and gradually becomes 1 at S_n=7.5. For approximating these available data by a representative curve that begins the transition at S_n =0.5 and ends at S_n=7.5, the following empirical relation is formed.

$$P_n = \left(1 - \left(\frac{0.75 - S_n}{0.25}\right)^{a_3}\right)^{a_4} \tag{17}$$

With this relation, $P_n = 0$ when $S_n = 0.5$ and $P_n = 1$ when $S_n = 0.75$. The path followed by the curve from 0 to 1 is determined by the coefficients, a_3 and a_4. In order to determine the coefficients that provide the best fit, the available data between the S_n ranges of 0.5 and 0.75 are fitted through a non-linear least squares algorithm in Matlab. The resulting values for the coefficients are a_3 = 0.52 (-0.3942, 1.424) and a_4 = 0.097 (0.007527, 0.1855). The confidence bounds for these parameters at 95% probability level are given in the parenthesis. This relation is valid for 0.5<S_n<0.75. For S_n <0.5, no percolation is found in the nano particles ($P_n = 0$) and for S_n >0.75, the nano particles are fully percolated ($P_n = 1$).

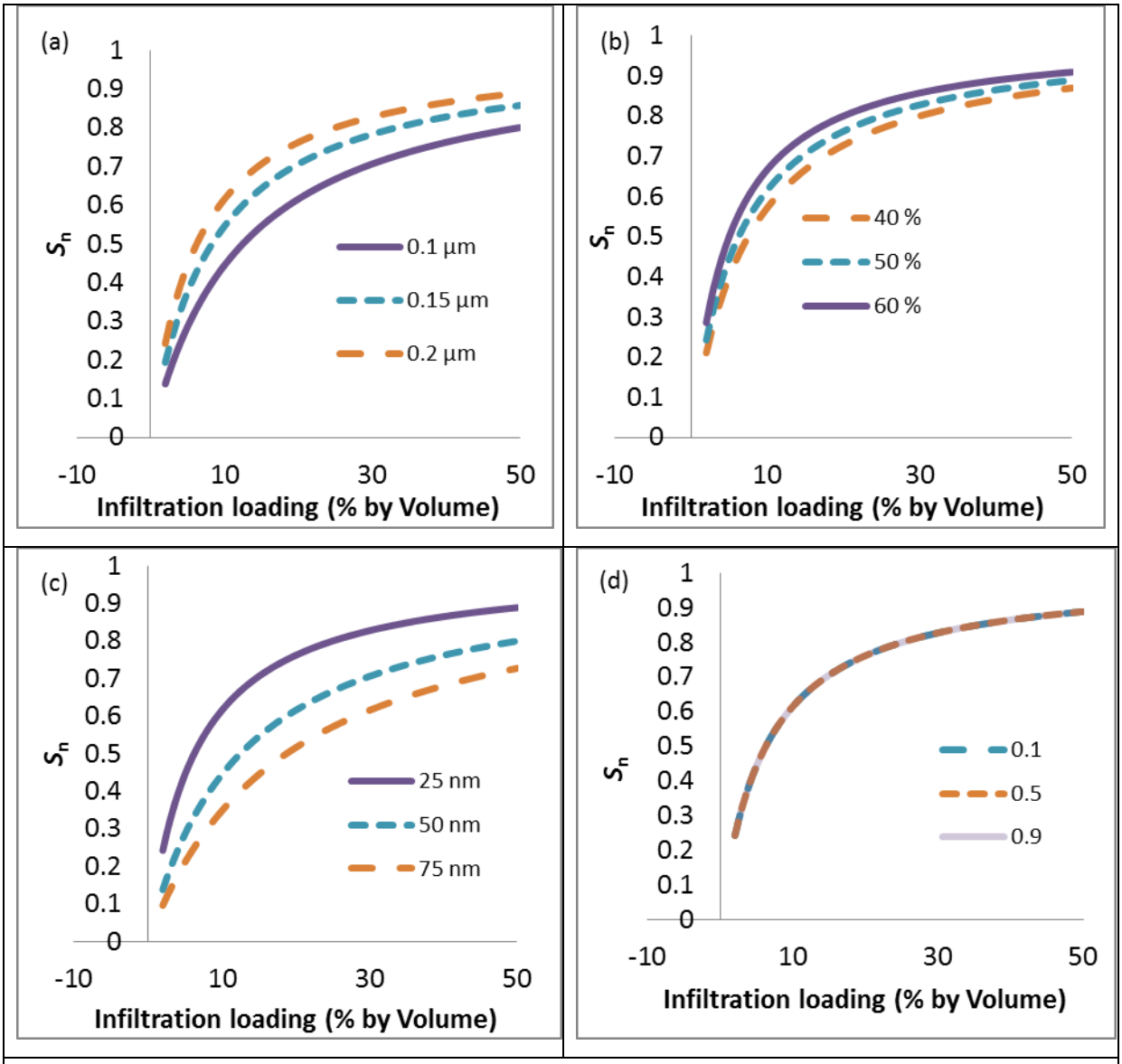

Fig. 2: Behaviour of the infiltrated particle surface area fraction for varying electrode microstructural parameters.

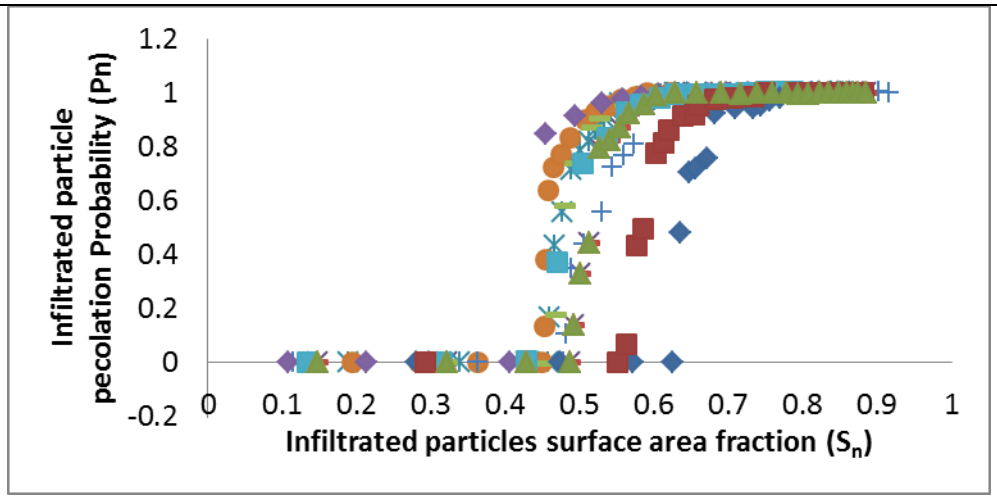

Fig. 3: Variation of the infiltrated particle percolation probability Vs its surface area fraction for all available cases from [8].

The pore percolation is a limiting variable at the higher ranges of the infiltration loading. Since the pore space is one of the phases that forms the TPB, unavailability of percolated pore spaces will result in the sudden fall of the TPB length even before all the pore space is occupied. From the numerical results presented in [8], we can conclude that pore percolation in the infiltrated electrodes is strongly sensitive to the backbone structure porosity and not very sensitive to the nano or back bone particle sizes or the agglomeration risk. Pore percolation is achieved earlier in an electrode with lesser backbone porosity compared to an electrode with a more porous backbone structure. The variable that can effectively reflect this behaviour is the electrode porosity calculated from Eq. 9. It can be seen from the plots in Fig. 4 that the electrode porosity has no effect on the particle sizes and the agglomeration. However the backbone structure porosity affects the electrode porosity such that the same infiltration loading will result in larger electrode porosity for an electrode with larger backbone porosity and vice versa. This is illustrated by Fig. 4b. Fig. 5 plots the pore percolation probability as a function of the electrode porosity for all available numerical data. The transition of the pore percolation probability from 0 starts roughly between the porosity values of 0.03 and 0.06 and gradually becomes 1 at $\phi = 0.2$. For approximating these available data by a representative curve that begins the transition at $\phi = 0.05$ and ends at $\phi = 0.2$, the following empirical relation is formed.

$$P_p = \left(1 - \left(\frac{0.2 - \phi}{0.15}\right)^{a_5}\right)^{a_6} \tag{18}$$

The best fit for the data is obtained with the values of a_5 =2.68 (0.8316, 4.518) and a_6 =0.25 (0.1399, 0.3681), where the 95% confidence intervals are given in the parenthesis.

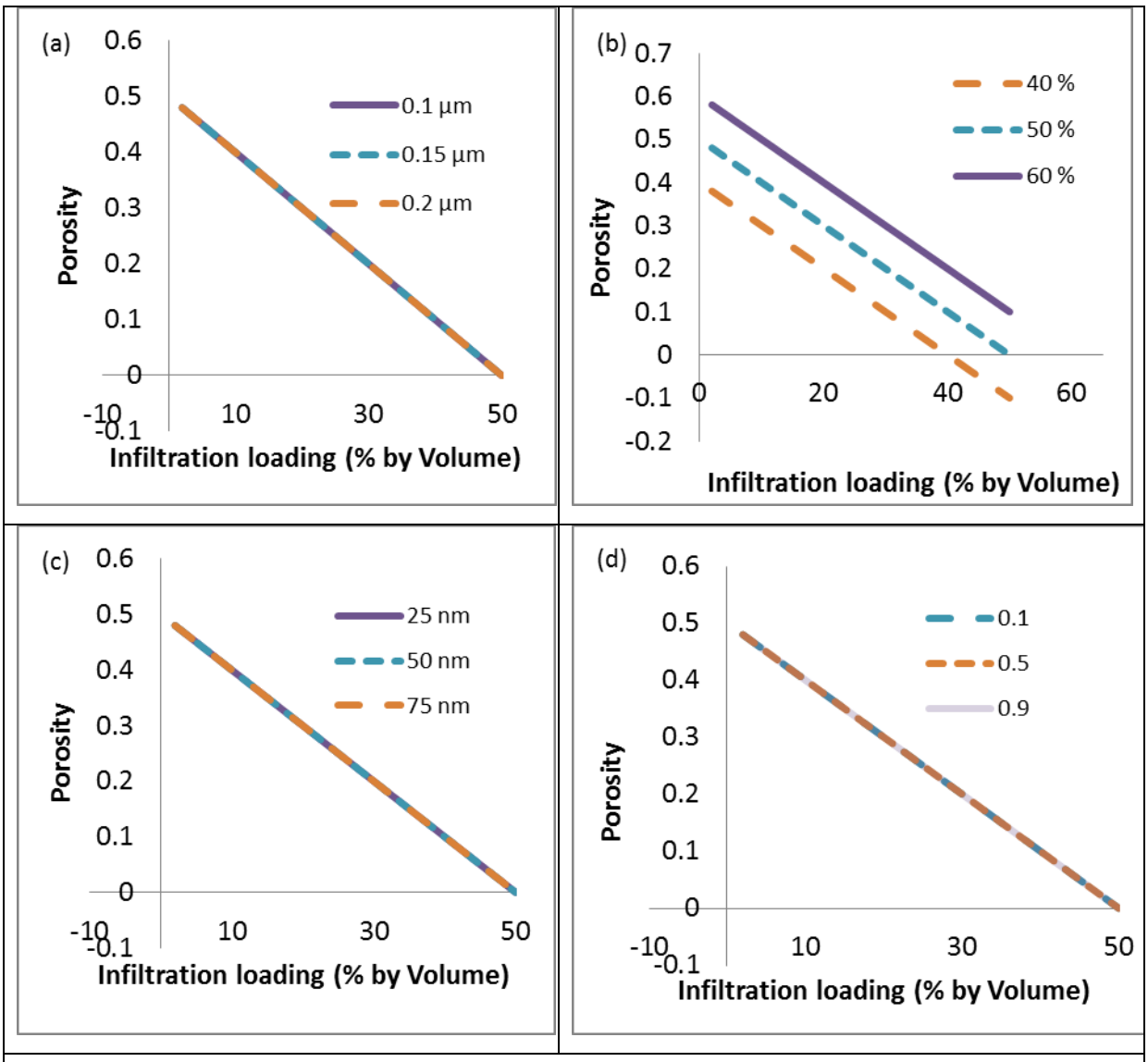

Fig. 4: Behaviour of the electrode porosity for varying electrode microstructural parameters.

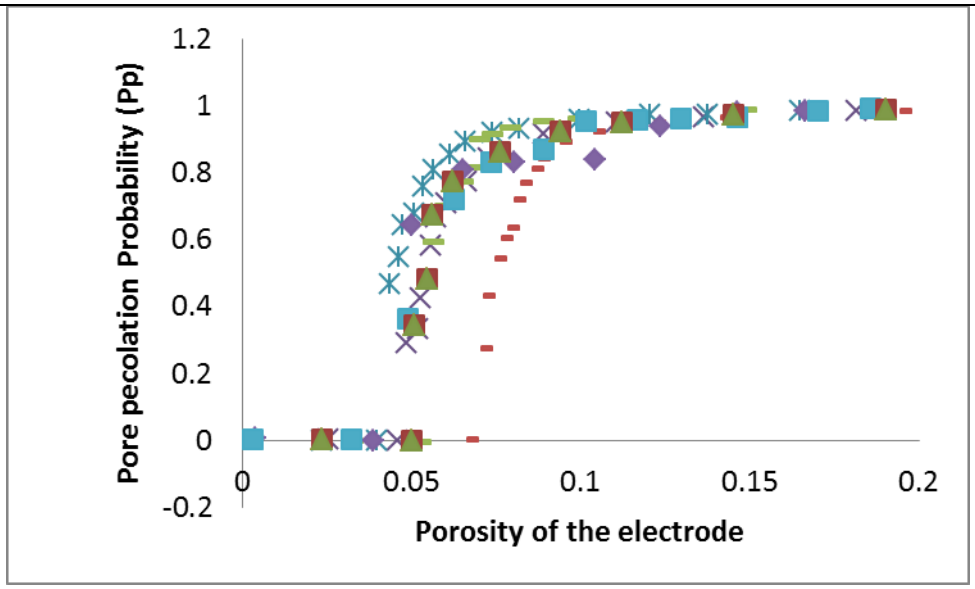

Fig. 5: Variation of the pore percolation probability Vs the porosity for all available cases from [8]

2.2. Parameter sensitivity

In order to evaluate the sensitivity of the model parameters a_1 to a_6, the effect of a small change in their values (+2 %) on the active TPB lengths are studied. The average percentage change in the active TPB length is reported in Table 2 for the conditions C1 to C6 whose microstructural parameters are listed in Table 1. To cover a wider space at each condition, the percentage change is calculated corresponding to four different values of the infiltrated particle volume fraction (0.15, 0.2, 0.25 and 0.3) and the average percentage changes in the active TPB lengths are reported in Table 2. Each row in the table presents the average percentage change in the active TPB lengths for different conditions resulting from the +2% change in the particular row parameter a_i. From the table, it is apparent that the parameter a_2 has the largest effect on the active TPB length and the smallest effect corresponds to parameter a_3. At condition C9, all parameters except a_2 have negligible effect on the output. The parameters a_5 and a_6 that define the pore percolation probability have almost no effect on the active TPB since their effect is restricted to a very narrow range of infiltration volume fractions that are not covered by the samples used.

Table 1: Conditions under which the parameter sensitivities are evaluated.

Conditions	r_B (μm)	r_n (μm)	w	ϕ_B (%)
C1	0.2	25e-3	0.9	50
C2	0.1	25e-3	0.9	50
C3	0.15	25e-3	0.9	50
C4	0.2	50e-3	0.9	50
C5	0.2	75e-3	0.9	50
C6	0.2	25e-3	0.5	50
C7	0.2	25e-3	0.1	50
C8	0.2	25e-3	0.1	40
C9	0.2	25e-3	0.1	60

Table 2: Average percentage changes in the active TPB lengths with + 2% change in parameters.

	C1	C2	C3	C4	C5	C6	C7	C8	C9
a1	-0.0556	-0.0592	-0.0566	-0.0592	-0.0649	-0.4266	-2.7620	-0.0555	-0.0558
a2	2.1172	2.2540	2.1540	2.2540	2.4718	2.4700	4.8135	2.1123	2.1249
a3	0.0294	0.1508	0.0675	0.1508	0.1751	0.0294	0.0294	0.0595	0
a4	-0.0254	-0.2403	-0.0755	-0.2403	-0.4189	-0.0254	-0.0254	-0.0571	0
a5	0	0	0	0	0	0	0	0.0895	0
a6	0	0	0	0	0	0	0	-0.0592	0

3. Results and discussion

The performance of the proposed model is compared with the numerical data from [8] in this section. The behaviour of the different coordination numbers are also studied to gain an insight into the possible physical phenomena that result in the observed behaviour. The behaviour of the coordination numbers with the change in the infiltration loading are

presented in Figs. 6 and 7. The nominal parameters used in obtaining the results in Fig. 6 are; $r_B = 0.2\ \mu\text{m}$; $r_n = 25\ n\text{m}$; $\phi_B = 50\%$; $w = 0.9$. For obtaining Fig. 7, each of the parameter is varied to obtain different plots with all others held at their nominal values. It can be observed that the coordination numbers follow different trends resulting in the overall average coordination number (*Z*) decreasing with the increase in the infiltration loading. Note that the expression for $Z_{n,B}$ (Eq. 5) has the term of number fraction of the infiltrated particles in the denominator. Therefore, the $Z_{n,B}$ is not strictly defined for zero infiltration loading. Since the values at or near zero infiltration loading is not practically useful, this should not be a major drawback.

The trends in the components of the coordination number can be explained as follows. With the increasing infiltration loading, the number of nano particles will increase, while the number of the backbone particles remains constant. Therefore, it is reasonable that the average number of the backbone particles that are in contact with a nano particle ($Z_{n,B}$) particle will decrease. The $Z_{n,n}$ shows a slight increase followed by a gradual decrease to the former levels. While, the increase is obvious the decrease is not. A possible explanation for this could be that the backbone structure offers a canvas for more structured packing of the nano particles that is not available once all surfaces are occupied. The behaviour of Z_n is a direct consequence of the trends of $Z_{n,B}$ and $Z_{n,n}$. $Z_{B,n}$ has a larger magnitude compared with other terms because of the large number of smaller sized nano (*n*) particles contacting the backbone particles (refer to Fig. 1). $Z_{B,n}$ increases with more number of nano particles available for contact with the backbone particle, but reaches a limit when all backbone particle sites are covered. The behaviour of Z_n reflects the $Z_{B,n}$ since the $Z_{B,B}$ is constant. These behaviours of Z_n and Z_B result in the overall coordination number gradually decreasing as the infiltration loading is increased. While there is no data to verify these predictions, we interpret them based on the TPB length model that largely agrees with the reported numerical data (as discussed in later sections).

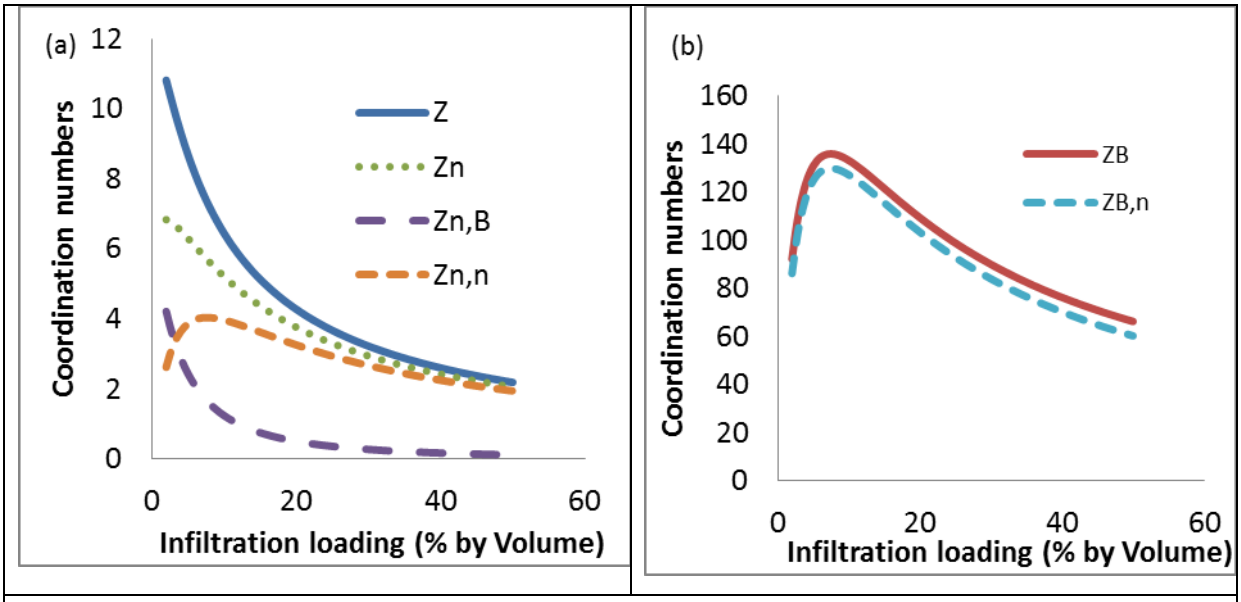

Fig. 6: The overall coordination number along with its different components.

In order to gain more insight into the coordination numbers, the behaviour of the $Z_{n,B}$ and Z with varying particles sizes, backbone porosities and w are plotted in Fig. 7. $Z_{n,B}$ follows the trend of the TPB length in that the smaller backbone particle size and the larger infiltrated particle size result in more contacts between the nano and the backbone particles and vice versa, throughout the infiltration loading range. It can also be seen from Fig. 7c that lower backbone porosity results in higher contacts and vice versa. Fig. 7d shows that larger agglomeration results in lesser contacts at lower infiltration loading but higher contacts at higher loading. The overall average coordination number (Z) also follows a similar pattern as seen in Fig. 8.

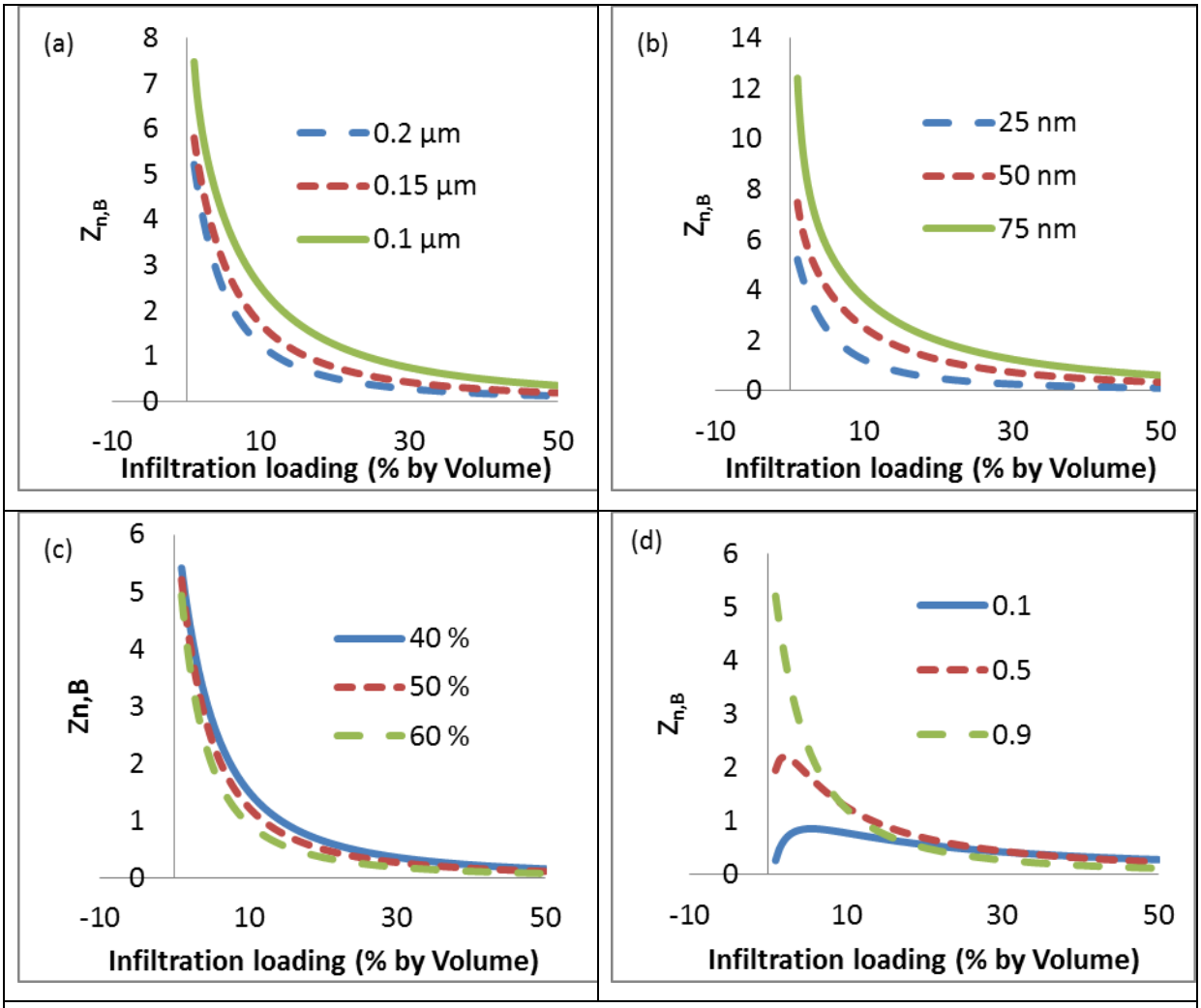

Fig. 7: Variation of $Z_{n,B}$ with different parameter ranges.

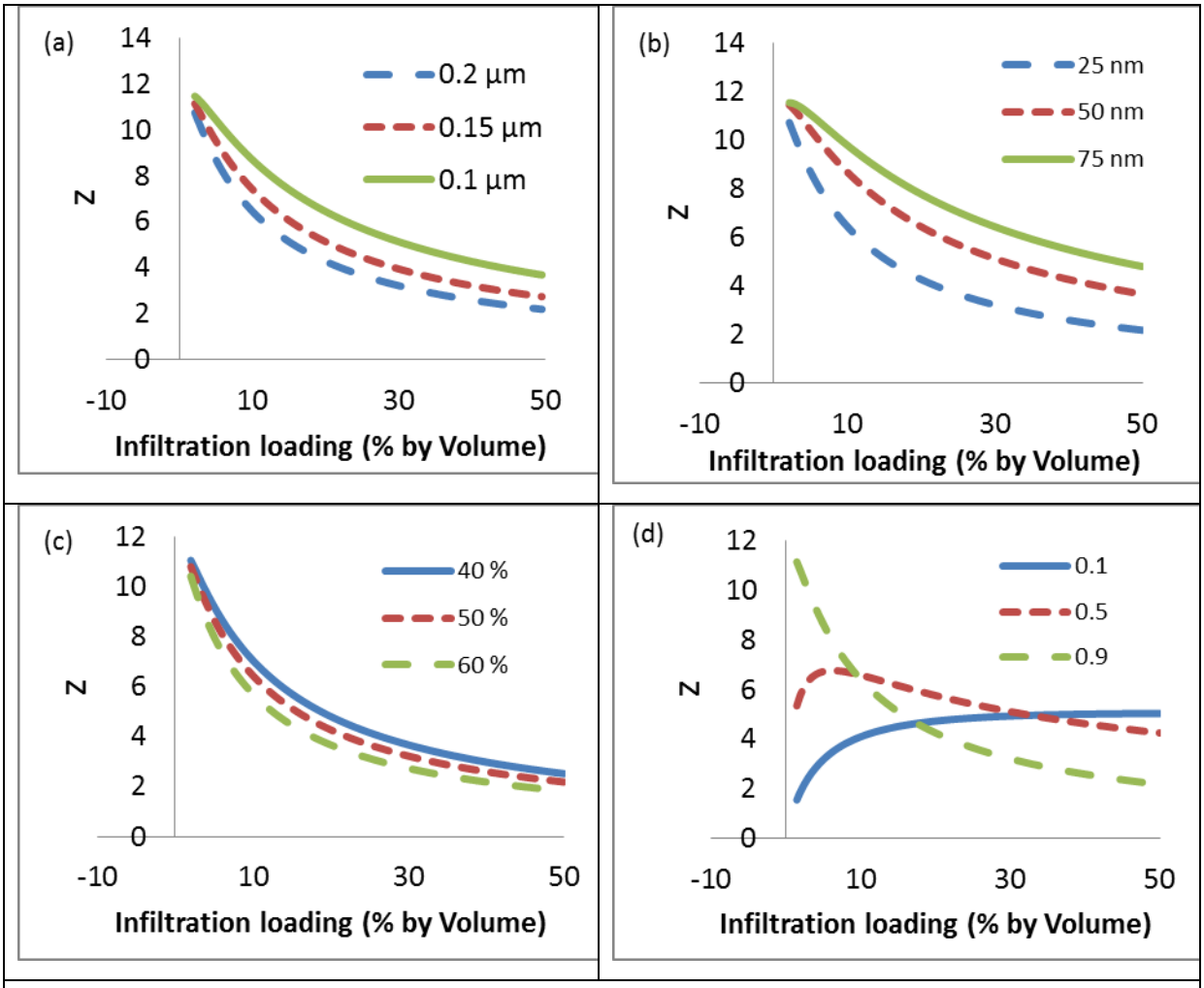

Fig. 8: Variation of Z with different parameter ranges.

3.1. Total TPB length per unit volume

The comparison of the total TPB lengths with [8] is provided in this section. The nominal parameters used in obtaining these results are: $r_B = 0.2\ \mu\text{m}$; $r_n = 25\ \text{nm}$; $\phi_B = 0.5$; $w = 0.9$. Each of the parameters is varied to obtain different plots with all the others held at their nominal values. In Fig. 9, the total triple phase boundary (TPB) lengths per unit volume are presented, where the lines represent the model results and the markers represent the numerical simulation results from [8]. The Fig. 9a presents the results corresponding to different diameters of the backbone particle. It can be seen that the total TPB lengths calculated by the model for 0.2 µm and 0.15 µm have a good fit with the numerical results. Although the trends are matching, the result for 0.1 µm has a discrepancy with the peak TPB lengths attained with a difference of around 3 % in the infiltration loading. The peak value of the TPB length has a much larger variation. It is interesting to note that the disagreement is

pronounced at lower values of the r_B / r_n ratio. This is also observed from the results in Fig. 9c, where the TPB length per unit volume is reported for different infiltrated particle sizes. The ratio of the radii is an important parameter in this system, and along with the agglomeration effect, highly influences the nano particle percolation [8]. The error is maximum at high agglomeration tendency (Fig. 9d) and low r_B / r_n ratios (Figs. 9a and 9c). So, it is reasonable that the origin of the error is the inability of the model to exactly capture the agglomeration phenomena. The effect is amplified at lower r_B / r_n ratios due to the relatively lower backbone particle surface area available for deposition. A sudden change in the slope is observed at around 40% infiltration loading in all the curves in the numerical simulation results, which is absent in our model results. Since these cannot be attributed to the pore percolation threshold phenomena (these results being total TPB lengths), it is not clear why these occur and no explanation was offered for this phenomenon in [8].

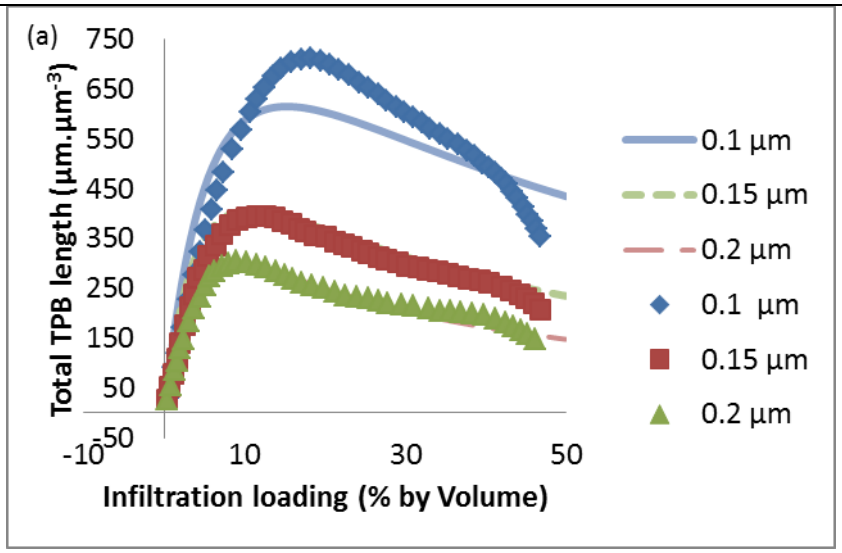

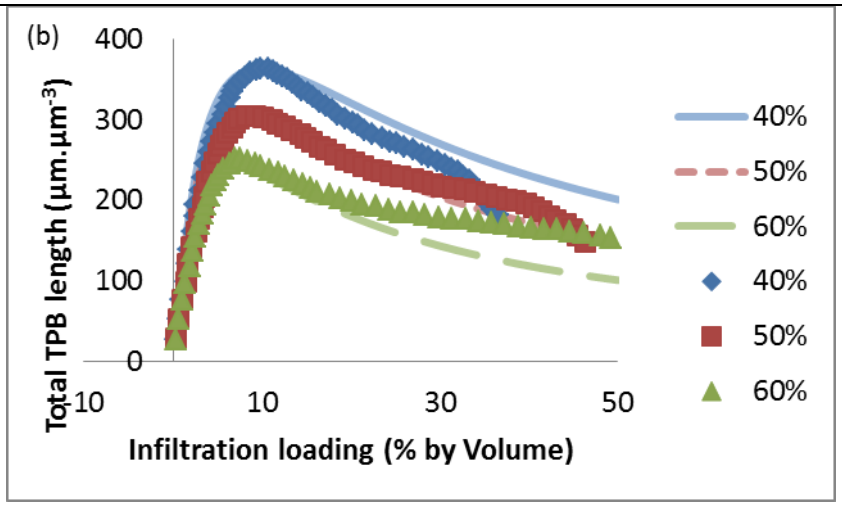

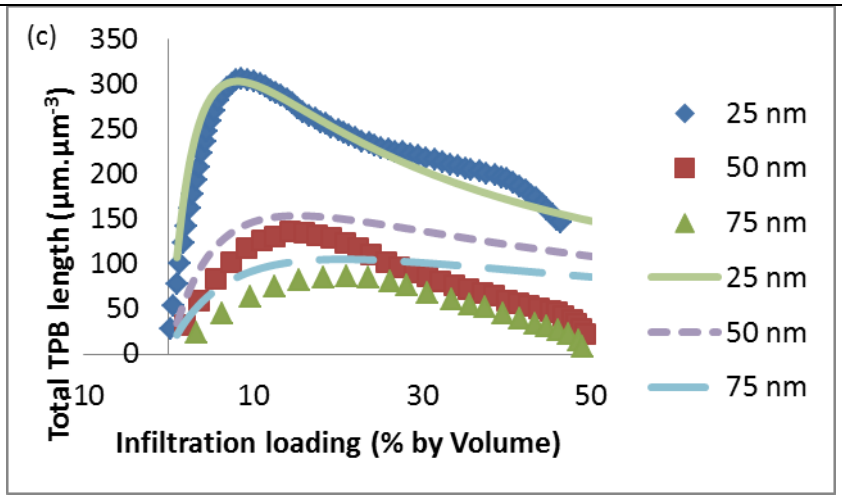

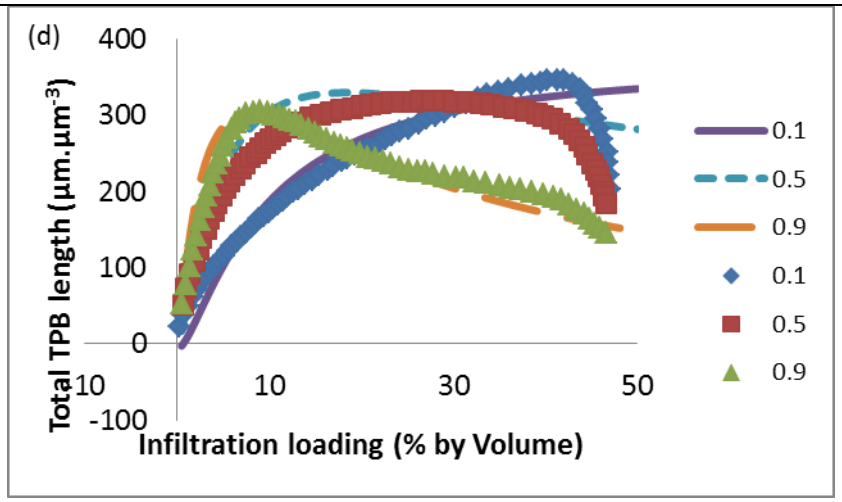

Fig. 9: Total TPB length per unit volume from the mathematical model compared with the numerical simulation results [8].

Fig. 9b shows the comparison of the numerical and modelled TPB lengths per unit volume corresponding to different backbone structure porosities. The agreement between the two cases is better compared to the previous case. The peak TPB length is correctly captured by the model. The disagreement at larger infiltration loadings may be due to the unexplained change in the slope which the model does not capture. In Fig. 9c, the TPB length plots are compared for varying radii of the nano particles. As before, the disagreement increases with lower r_B / r_n ratios, which may be attributed to the inability of the model to correctly capture the agglomeration effect. The plots of the model and numerical results for the TPB length for different values of w are presented in Fig. 9d. Since there is reason to believe that the agglomeration phenomena is not sufficiently represented, enhanced models for the

agglomeration effect in the infiltrated electrodes are required. For this, a thorough understanding of the agglomeration phenomena is necessary.

3.2. Active TPB length per unit volume

The total TPB length per unit volume considers only the contacts between the electronic and ionic conductors. However for effective conductive paths, the percolation of the conductors as well as the pore space is required. The backbone structure is fully percolated as it is pre-fabricated. Therefore, only consideration for the infiltrated particle percolation and the pore percolation is needed for calculating the active TPB length per unit volume. These are accounted in the model using the percolation probabilities defined in Section 2.1, which result in the plots in Fig. 10.

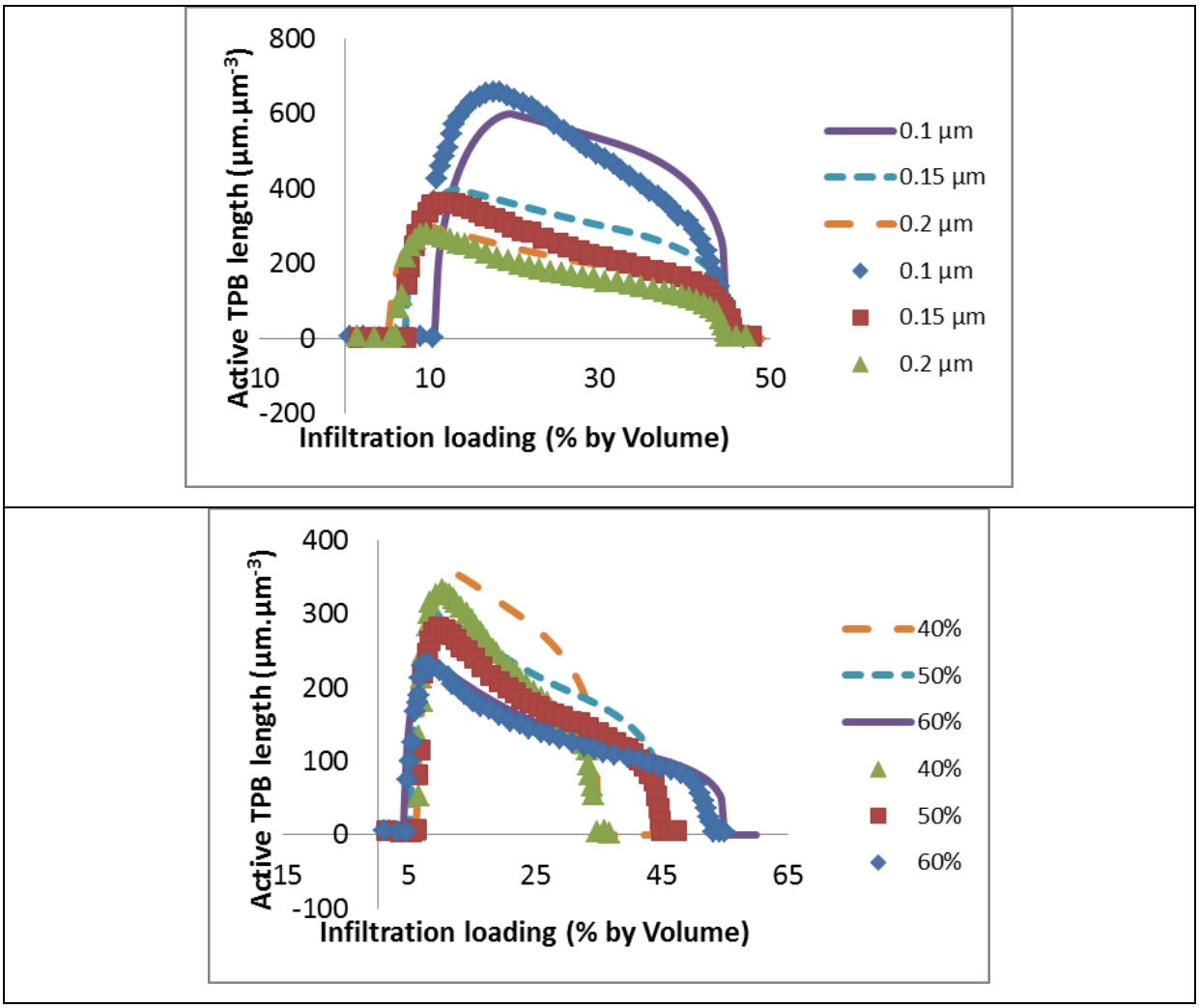

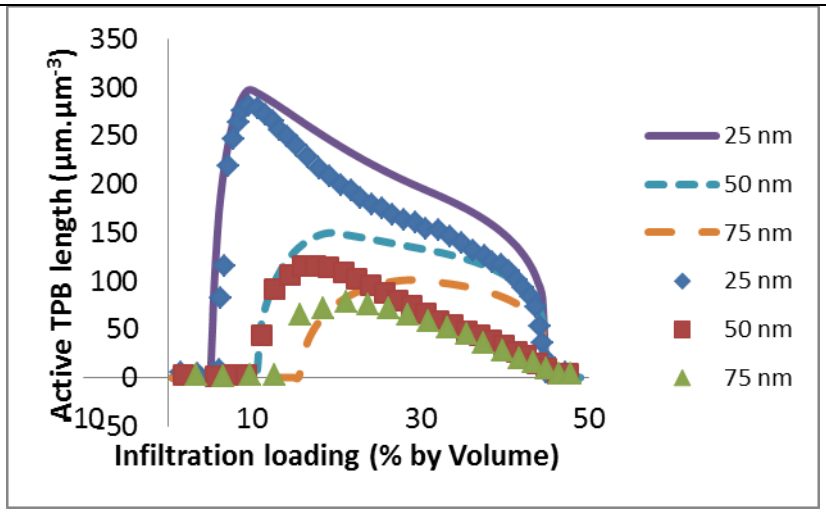

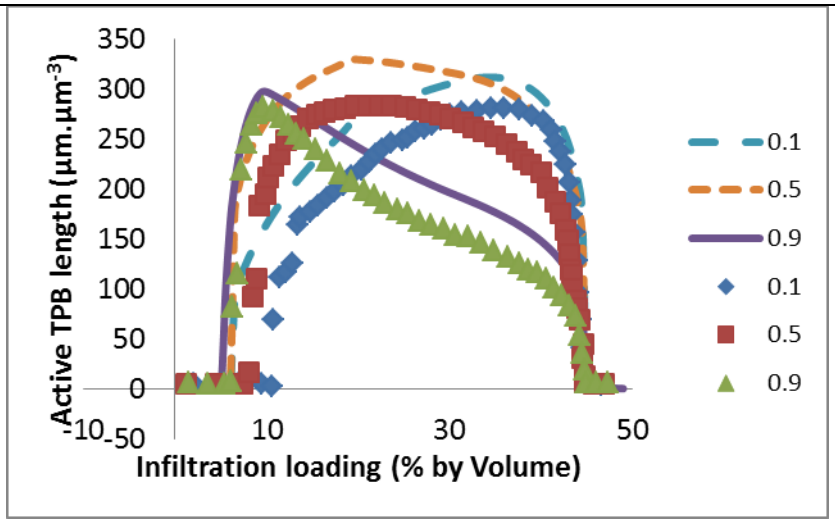

Fig. 10: Active TPB length per unit volume from the mathematical model compared with the numerical simulation results [8].

In the Fig. 10a, the active TPB lengths for different radii of the backbone particle are presented. The lines are the model results and the markers are the numerical simulation results from [8]. While the pore percolation threshold is represented accurately, the infiltrated particle percolation thresholds are a little offset for lower radii cases. Also, the inclusion of the percolation probabilities has slightly distorted the TPB curve at the mid ranges of infiltration loading. In the case of varying backbone porosities (Fig. 10b), the infiltration and the pore percolation thresholds are reasonably accurate, while the distortion is observed at mid ranges of the infiltration loading. This distortion is more with lower backbone porosity. In the case of varying nano particle diameters (Fig. 10c), the pore percolation thresholds are captured correctly, whereas there is some error in the infiltration

thresholds at larger particle radii. The infiltration percolation relation is not capable of capturing the nano particle percolation behaviour with the variation of w as discussed in Section 2.1. This is also clear from Fig. 10d.

3.3. Analysis for constant electrode porosity

An alternate analysis, where the electrode porosity is constant (50%), is conducted and the results for the total and active TPB lengths are plotted in Figs. 11 and 12. For the sake of comparison, also included in the plots are the results for the case of fixed backbone porosity. The lines in these plots represent the fixed backbone porosity case and the markers represent the constant electrode porosity case. From these figures, it is clear that for all the cases considered, the peak TPB length is smaller for the constant electrode porosity case compared with the fixed backbone porosity case. In addition, the TPB length peaks occur at a lesser infiltration loading in all the cases.

The larger peak TPB length in the case of fixed backbone porosity can be explained as follows. In the case of fixed backbone porosity, the actual electrode porosity continuously decreases as the infiltration loading is increased (refer Fig. 4). For example, at the point where the peak TPB length is obtained, the electrode porosity is actually about 40 % for the case of the 0.2 μm backbone particle radius as can be seen from Figs. 4 and 11a. On the other hand, the electrode porosity remains same in the constant electrode porosity case. This means that there are more number of particles in the fixed backbone porosity case compared to the other case and hence the increased TPB length.

The peak in the TPB length occurs because beyond certain infiltration loading, the nano particles have a lesser chance to contact the backbone particles. In the constant electrode porosity case, the number of backbone particles decreases with the increasing infiltration loading; whereas the backbone particle number is constant in the fixed backbone porosity case. Due to this reduction in the number of the backbone particles with infiltration loading, the peak TPB length occurs earlier in the constant electrode porosity case compared to the fixed backbone porosity case. The active TPB lengths for the constant electrode porosity case are plotted for the different parameter values and compared to the fixed backbone porosity case in Fig 12. The lines in these plots represent the fixed backbone porosity case

and the markers represent the constant electrode porosity case. It can be seen that the trends of the active TPB lengths are similar to the total TPB length's trends.

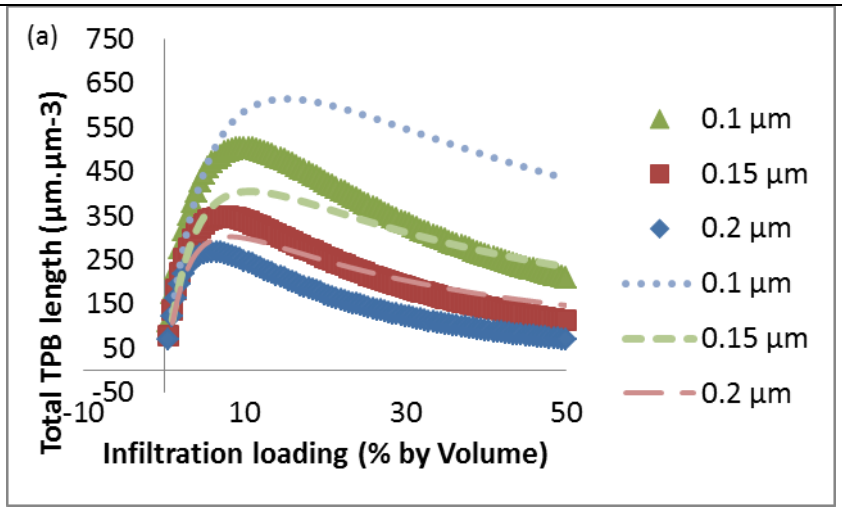

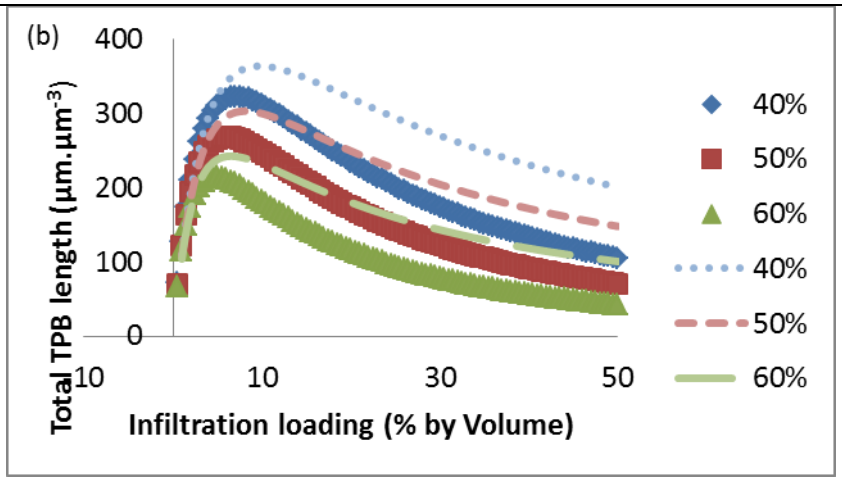

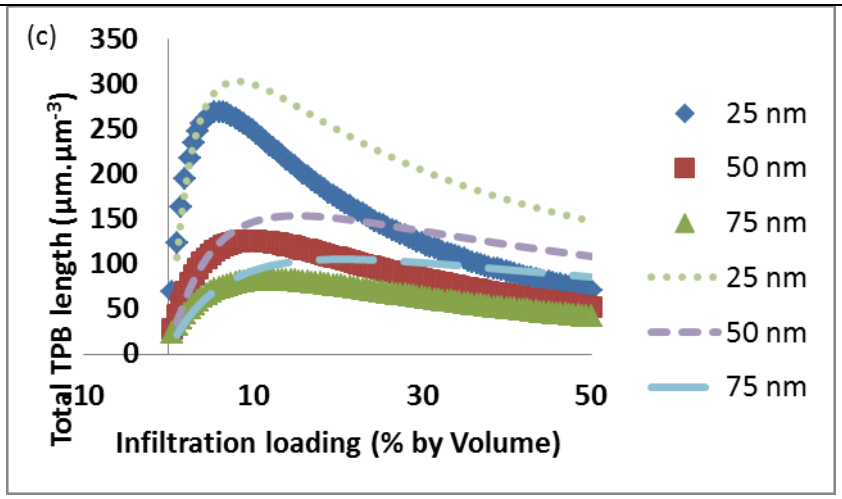

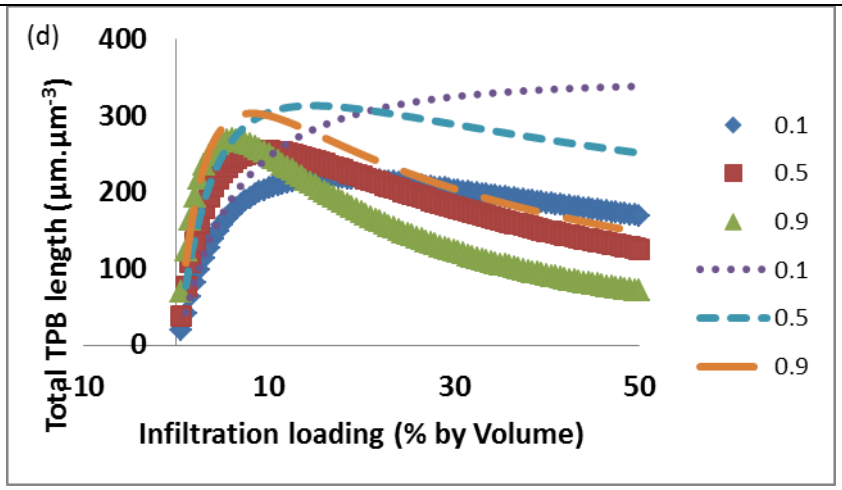

Fig. 11: Total TPB length per unit volume from the constant electrode porosity case compared with the fixed backbone porosity case.

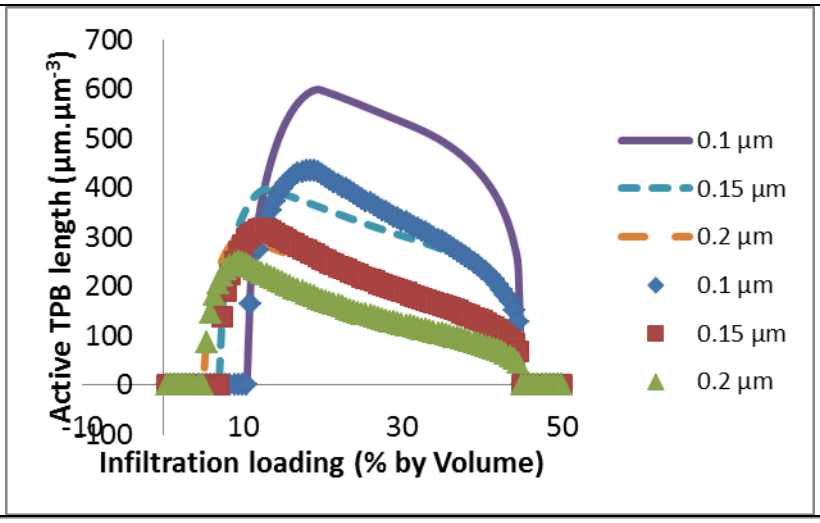

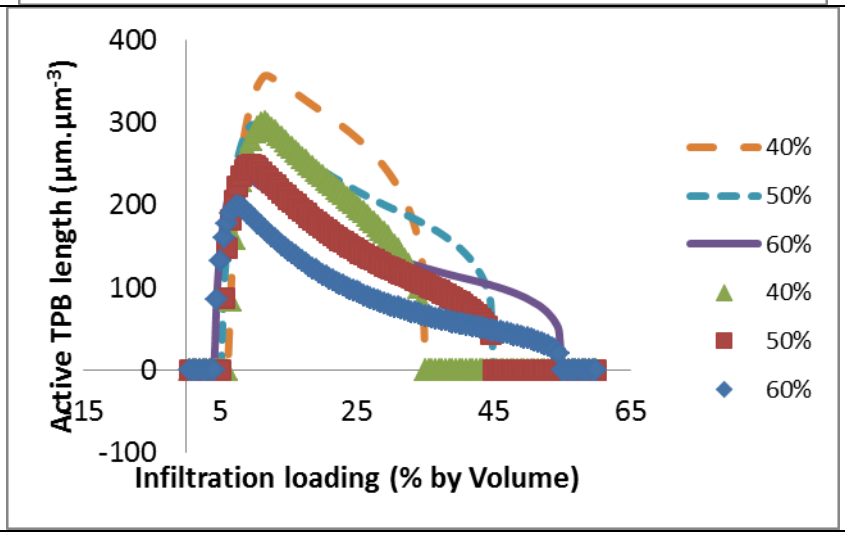

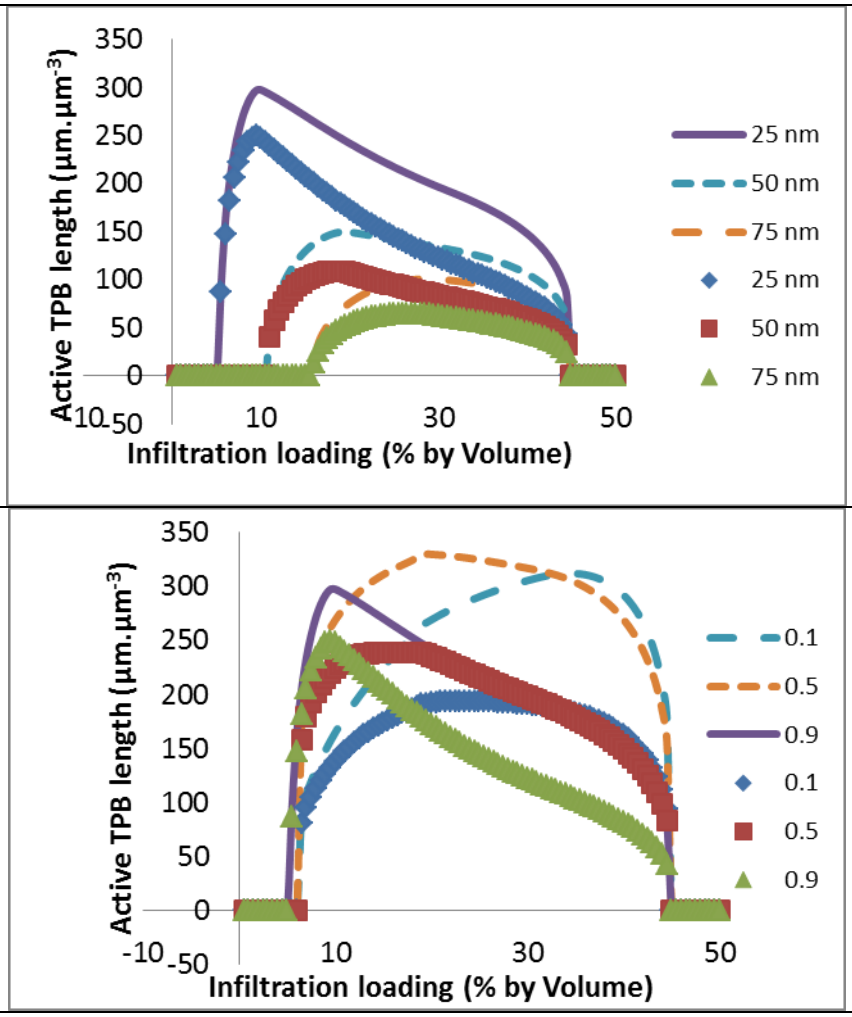

Fig. 12: Active TPB length per unit volume from the constant electrode porosity case compared with the fixed backbone porosity case.

3.4. Comparison with other models and experimental data

In this section, the proposed model is compared with other models for infiltrated electrodes in the literature and available experimental data on the TPB lengths. A numerical simulation of the microstructure of infiltrated electrodes is reported in [16], in which the whole process of electrode fabrication including sintering is simulated. Direct comparison with this work is not possible as the particle size ratios are specified in terms of pre-sintering conditions. However, our model results agree qualitatively with the results from [16].

A model for the infiltrated electrodes was proposed in [11] based on geometric arguments. The assumptions included that the backbone particles are coated with a single layer of nano particles of the other phase and that the infiltrated particles are much smaller than the backbone particles ($r_n/r_B \leq 0.1$). Given the backbone porosity, the number of backbone particles can be evaluated. The number of the nano particles followed from geometric

arguments about the single layer of nano particle coverage on the backbone particles. It is clear from Eq. 21 that given the particle size and number ratios, the volume fraction ratio is fixed. This relation is obtained by considering the definition of the number fractions in Eqs. 19 and 20. Therefore, this model does not support the specification of the particle volume fractions independent of their sizes and hence has limited applicability. With this model [11], it is not possible to evaluate the dependence of the TPB length on the infiltration volume fraction as desired for design optimisation.

$$\zeta_n = \frac{\psi_n / r_n^3}{\left(\psi_n / r_n^3\right) + \left(\psi_B / r_B^3\right)} \tag{19}$$

$$\zeta_n = \frac{\psi_B / r_B^3}{\left(\psi_n / r_n^3\right) + \left(\psi_B / r_B^3\right)} \tag{20}$$

$$\frac{n_n}{n_B} = \frac{\psi_n r_B^3}{\psi_B r_n^3} \tag{21}$$

Comparison of the results from the Zhu et al. model [11] and our model is shown in Fig. 13. For the comparison, the particle numbers corresponding to the size ratios are calculated using the Zhu et al. model [11], which is then used to calculate the volume fractions for each of the cases in Fig. 13. The backbone particle volume fractions that are used in our model for comparison in Fig. 13 are 0.6958 for Figs. 13a1, 13b1 and 13c1, 0.8345 for Figs. 13a2, 13b2 and 13c2, and 0.9305 for Figs. 13a3, 13b3 and 13c3. The backbone structure porosity for plots Fig. 13a1, 13a2 and 13a3 is 40%, that for Figs. 13b1, 13b2, 13b3 is 50% and that for Figs. 13c1, 13c2, 13c3 is 60 %. The agglomeration w is taken as 1 corresponding to the percentage coverage of 1 used for the Zhu et al. model [11]. From Fig. 13, we can conclude that our model can reproduce the results of Zhu et al. model [11] fairly well except at low backbone particle volume fractions. The deviation increases with the decrease in the r_n/r_B ratio. Given that the volume fractions are fixed, a smaller r_n/r_B ratio implies a smaller number of relatively large backbone particles and a larger number of relatively small infiltrated particles, which increases the number of contacts between the two particle types. In the work of Zhu et al. model [11], 15^o contact angle is assumed between the backbone and the nano particles rather than the 90^o that is more realistic [8]. This difference in the contact angle can explain the observed deviation, which is amplified at low r_n/r_B ratios due to more number of contacts.

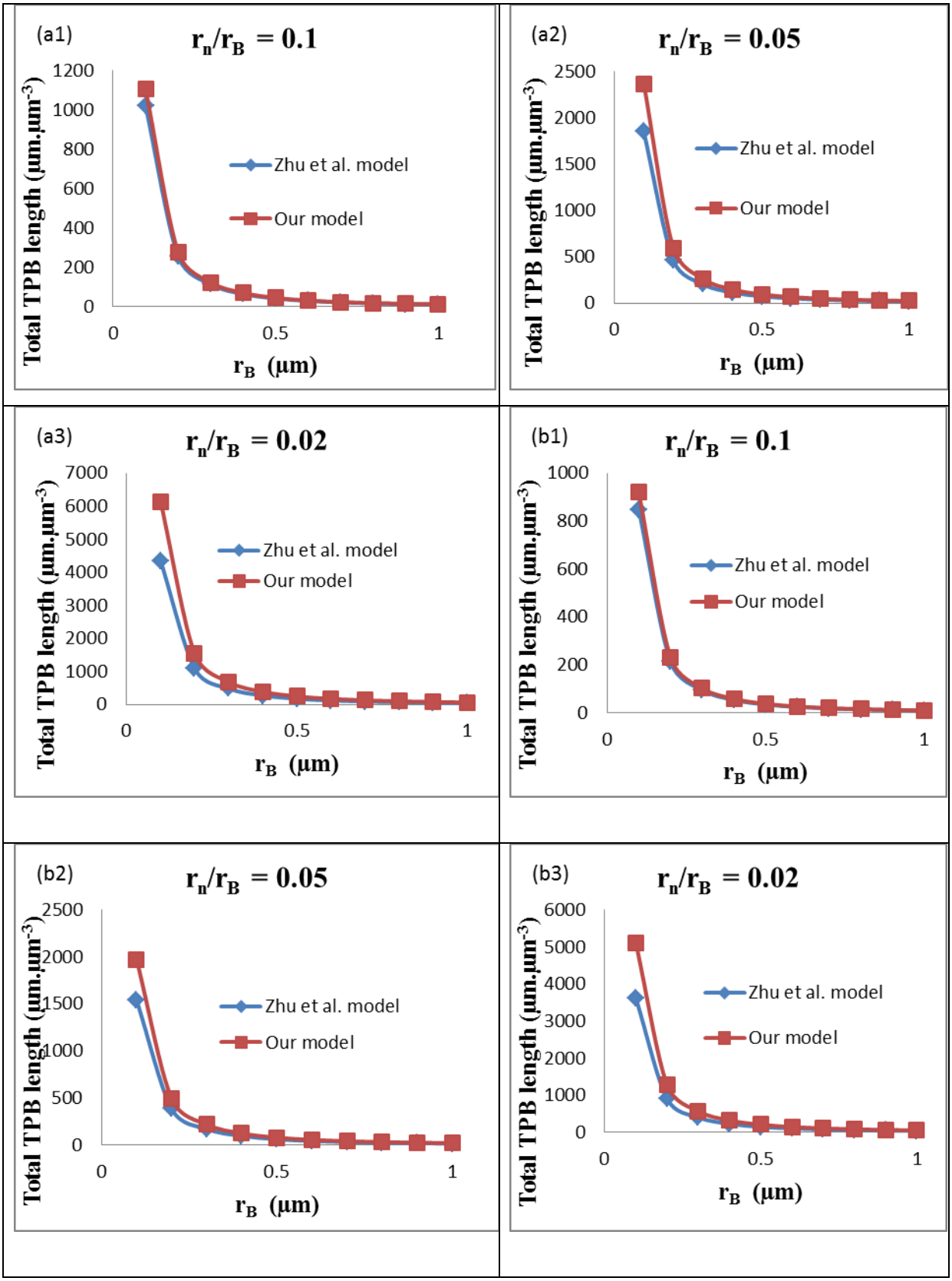
(a1)
$r_n/r_B = 0.1$
Total TPB length (μm.μm^{-3})
1200
1000
800
600
400
200
0
0
0.5
1
r_B (μm)
Zhu et al. model
Our model
(a2)
$r_n/r_B = 0.05$
Total TPB length (μm.μm^{-3})
2500
2000
1500
1000
500
0
0
0.5
1
r_B (μm)
Zhu et al. model
Our model
(a3)
$r_n/r_B = 0.02$
Total TPB length (μm.μm^{-3})
7000
6000
5000
4000
3000
2000
1000
0
0
0.5
1
r_B (μm)
Zhu et al. model
Our model
(b1)
$r_n/r_B = 0.1$
Total TPB length (μm.μm^{-3})
1000
800
600
400
200
0
0
0.5
1
r_B (μm)
Zhu et al. model
Our model
(b2)
$r_n/r_B = 0.05$
Total TPB length (μm.μm^{-3})
2500
2000
1500
1000
500
0
0
0.5
1
r_B (μm)
Zhu et al. model
Our model
(b3)
$r_n/r_B = 0.02$
Total TPB length (μm.μm^{-3})
6000
5000
4000
3000
2000
1000
0
0
0.5
1
r_B (μm)
Zhu et al. model
Our model

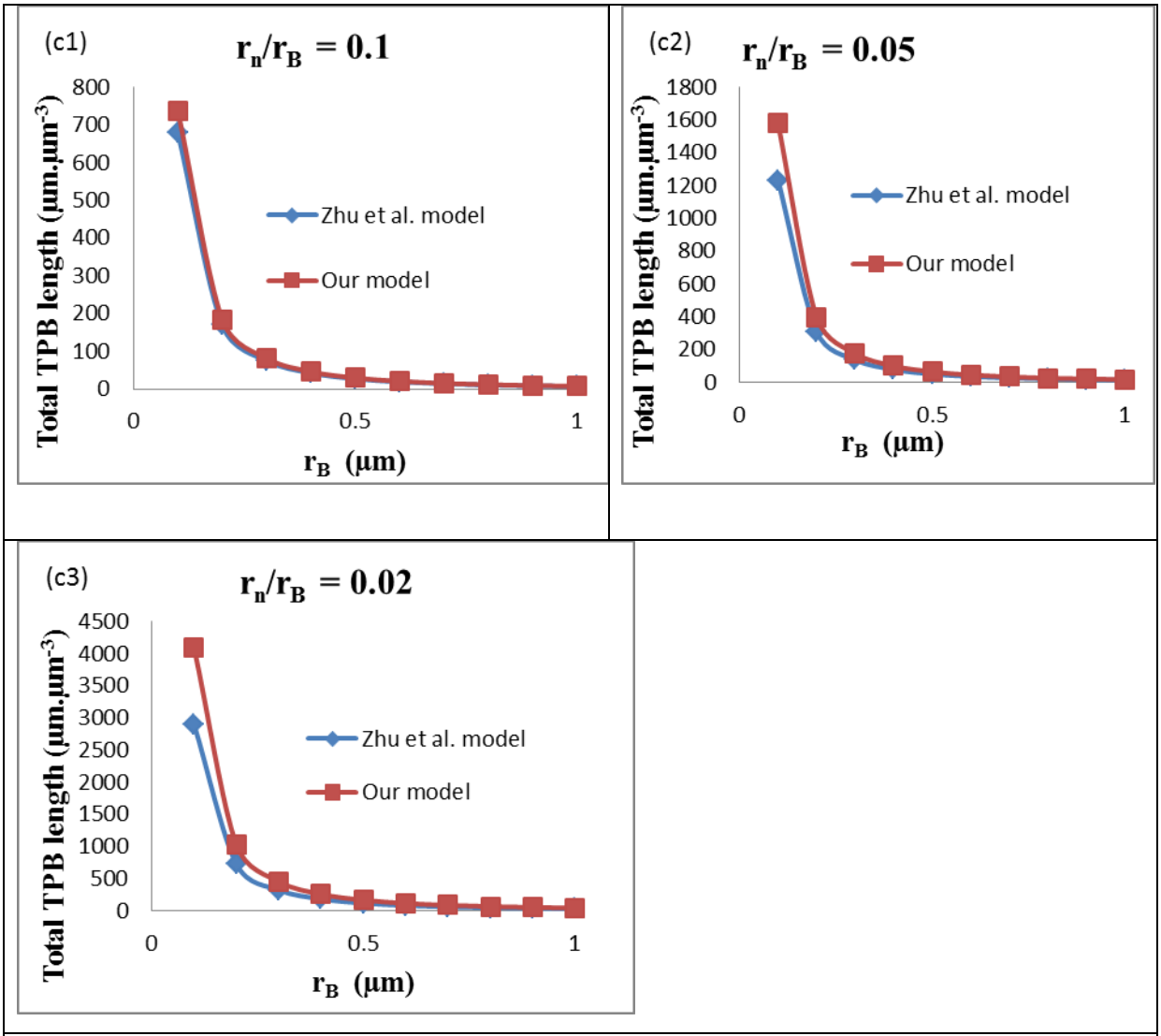

Fig. 13: Model comparison with the model of Zhu et al. [11] at different backbone structure porosities.

Zhang and Xia [17] expanded the geometry based formulation of Zhu et al. model [11] to derive an expression for the coordination number $Z_{B,n}$ which is then used to define the TPB length. The drawback with the $Z_{B,n}$ derived from geometric considerations is that it will depend only on the particle size ratio and not on the volume fractions of the particles. In their work, the electrode is considered fully percolated with the percolation probability of 1. Further the contact angle in the infiltrated particles is considered 15^{o} like in Zhu et al. model [11]. However, the number of particles is formulated in terms of the overall electrode porosity (as in Eqs. 15 and 16), thereby involving the volume fractions in the TPB calculation. The comparison of our model results with the Zhang and Xia model [17] is presented in Fig.

14. The particle sizes in generating the plots are r_n = 25e-3 µm; r_B = 0.2 µm. Since $Z_{B,n}$ is constant given the particle sizes in the Zhang and Xia model [17], the variation in the TPB length only depends on the particle numbers. The under prediction of the TPB length at low volume fractions of the infiltrated particles may be due to the lesser contact angle considered in the model. At higher volume fractions of the infiltrated particles, the number of contact points between the particles should come down due to the lesser number of backbone particles. Since this is not reflected in the model Zhang and Xia model [17] ($Z_{B,n}$ remaining constant), we see an over prediction of the TPB length. In other words, the geometric assumption of a single layer of nano particle covering the backbone particles results in imposing constraints on accommodating any volume fraction and particle radii combination.

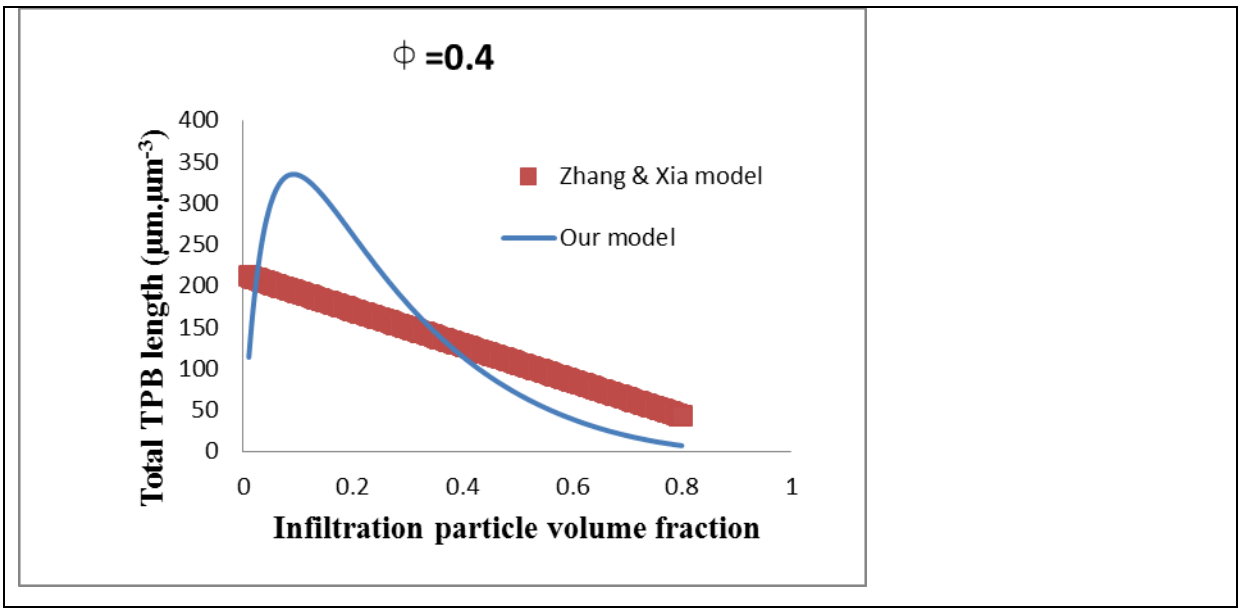

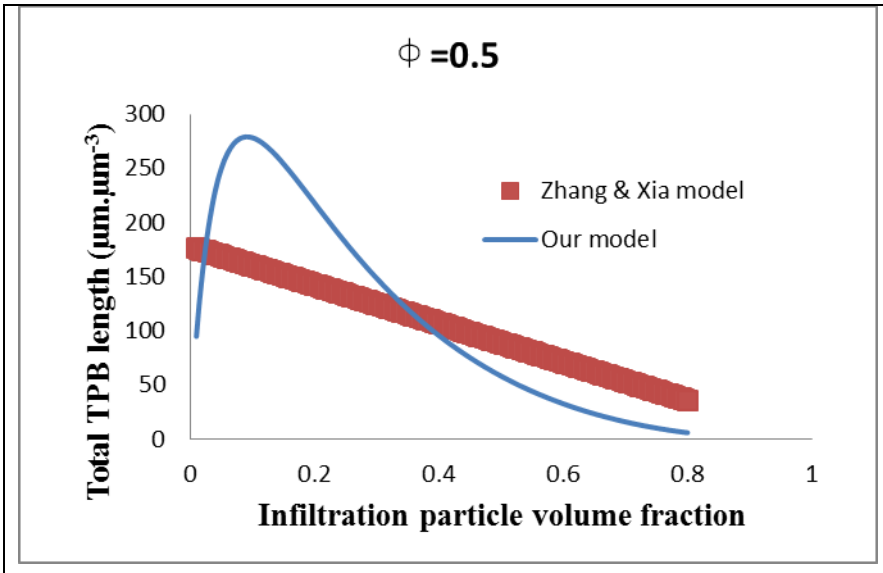

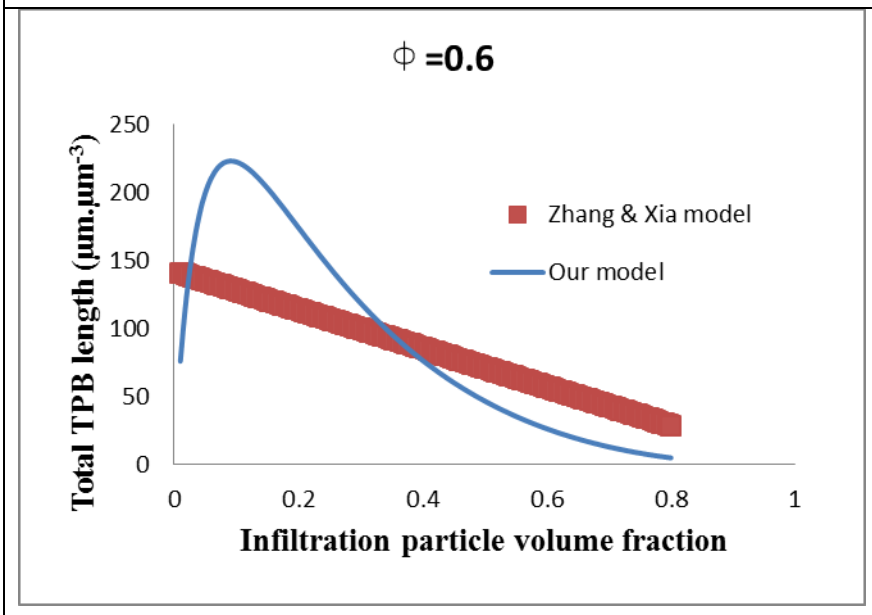

Fig. 14: Model comparison with results of Zhang and Xia model [17].

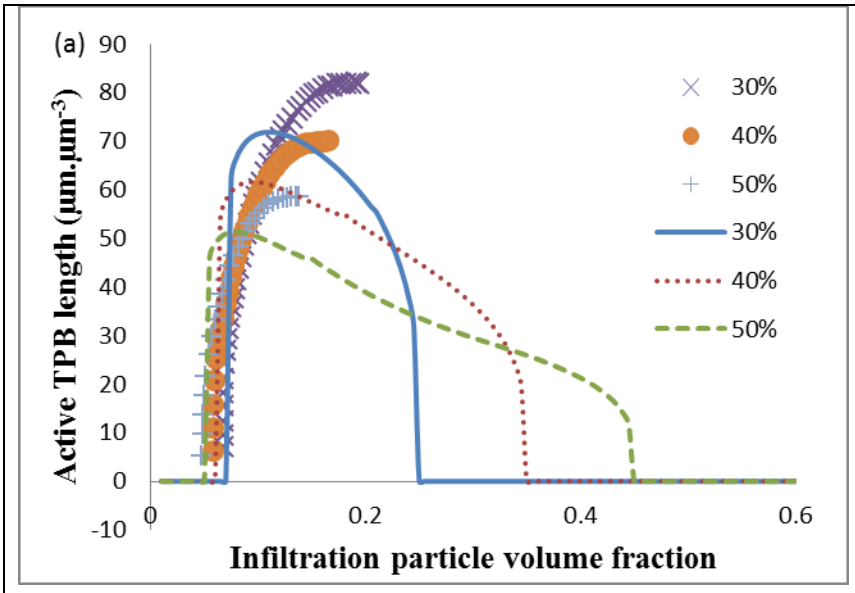
(a)
Active TPB length (μm.μm-3)
90
80
70
60
50
40
30
20
10
0
-10
0
0.2
0.4
0.6
Infiltration particle volume fraction
30%
40%
50%
30%
40%
50%

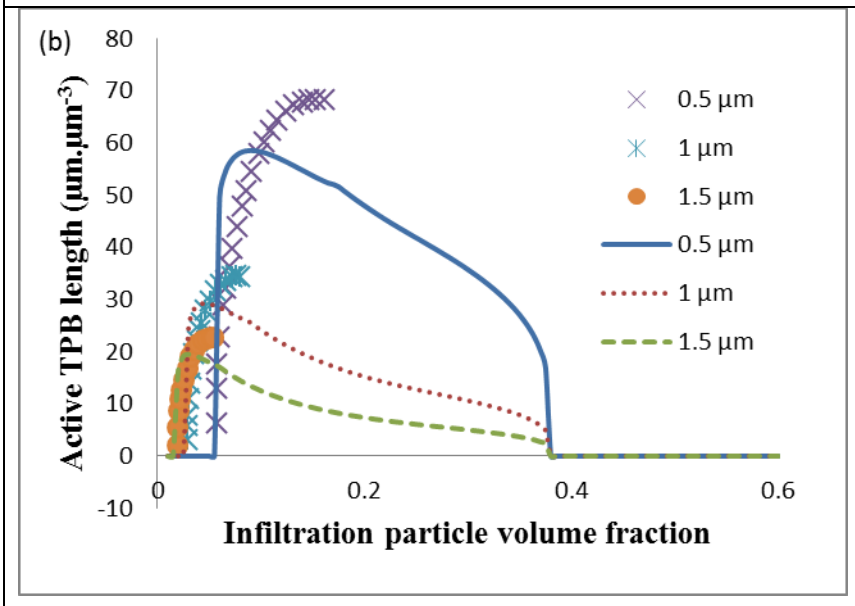
(b)
Active TPB length (μm.μm-3)
80
70
60
50
40
30
20
10
0
-10
0
0.2
0.4
0.6
Infiltration particle volume fraction
0.5 μm
1 μm
1.5 μm
0.5 μm
1 μm
1.5 μm

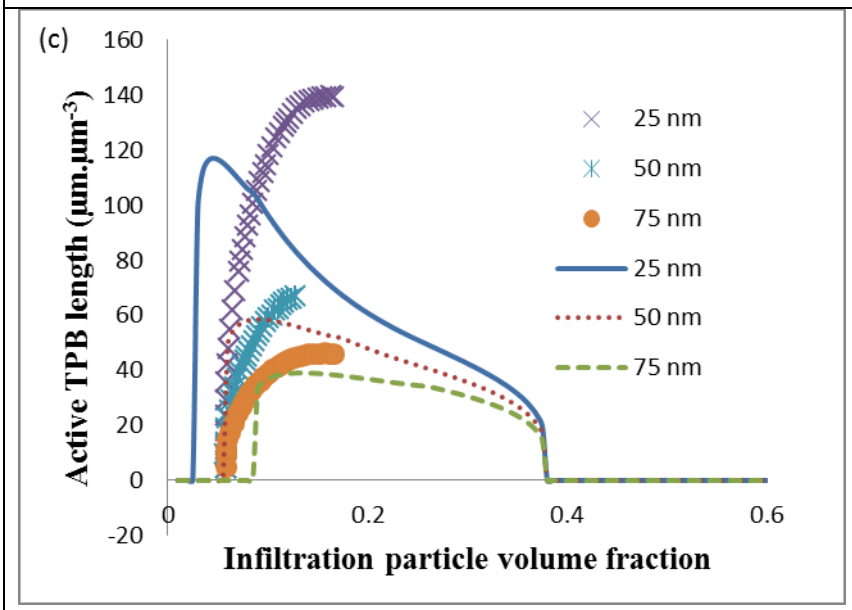
(c)
Active TPB length (μm.μm-3)
160
140
120
100
80
60
40
20
0
-20
0
0.2
0.4
0.6
Infiltration particle volume fraction
25 nm
50 nm
75 nm
25 nm
50 nm
75 nm

Fig. 15: Model comparison with results of Hardjo et al. model [1].

Another model presented in Hardjo et al. [1] is based on evaluating the site occupation probability of the nano particles based on the measured effective conductivity of the electrodes. The results from this model are compared in Fig. 15, where the lines represent our model results and the markers represent the Hardjo et al. model [1] results. The porosity values used in the generation of Figs. 15b and 15c is 43 %. It can be seen that the Hardjo et al. [1] model over-predicts the active TPB lengths compared to our model. Since the effective conductivity used in the Hardjo et al. model [1] is not mentioned, the reason for the mismatch is not clear. However, it can be seen from the figures that the infiltrated particle percolation thresholds for the models agree except for the varying infiltrated particle size case in Fig. 15c.

The model predictions for the TPB lengths were compared with the experimental results for the infiltrated electrodes reported in [18]. In [18], two infiltrated electrodes are studied; one with one time infiltration and the second with 10 times infiltration. These are named Ni (1) – GDC and Ni (10) – GDC, respectively. The microstructural parameters and the TPB lengths are tabulated in Table 3. For our model simulation, w is treated as an adjustable parameter as the agglomeration extent in the experimental work is unknown. The predictions of our model with w=0.43 are close to the experimentally evaluated TPB lengths for both infiltration cases, providing some degree of confidence in the model.

Table 3: Model predicted and experimental TPB lengths for two different electrode compositions

		Ni (1) - GDC	Ni (10) - GDC
Volume fraction (%)	Ni	1.29	19.8
	GDC/YSZ	56.9	60.2
	Pore	41.8	20.1
Particle size (μm)	Ni	0.102	0.354
	GDC/YSZ	0.748	0.706
Experimental TPB length ($\mu m\ \mu m^{-3}$)		11	18.4
Our model TPB length ($\mu m\ \mu m^{-3}$)		11.8915	17.8547

4. Conclusions

A model for calculating the TPB lengths in infiltrated electrodes is presented. This model is based on the basic structure offered by the principles of coordination numbers and the percolation theory concepts. An expression for the overall average coordination number as a function of the changing particle composition in the infiltrated electrodes is proposed that enables the calculation of the TPB lengths. Correlations for the percolation probabilities are developed based on the behaviour of certain key variables in the system. The model predictions are compared with the numerical model results for the different backbone and nano particle sizes, backbone porosities and the agglomeration effect. Comparisons are also provided with other analytical models in the literature and reasons for observed deviations are discussed. The model is further validated with experimentally measured TPB lengths for two different compositions of the infiltrated electrodes. The behaviour of the different component coordination numbers that lead to the predicted characteristic of the TPB length are studied. The model suggests that the overall average coordination number of the infiltrates electrode decreases as the infiltration loading is increased. To demonstrate the applicability of the model, an alternate analysis with fixed electrode porosity and varying nano and backbone particle compositions is presented.

Acknowledgements:

The authors acknowledge the Australian Research Council (ARC) for the discovery project grant DP150104365.

Nomenclature

$Z_{x,y}$	Average number of y particles in contact with an x particle
Z_x	Average number of contacts between an x particle and neighbouring particles of all types
ψ_x	Volume fraction of x particles relative to the total solid volume
S_x	Surface area fraction of all x particles

r_x	Radius of all x particles
ζ_x	Number fraction of x particles
V	Volume
n_x	Number of particles of type x
Z	Overall average coordination number of all particles
λ	TPB length per unit volume
P	Percolation probability

Subscripts

n	Nano or the infiltrated particle
B	Backbone particle
act	Actual
p	Pore
el	Electronic
io	Ionic

References

[1] Hardjo EF, Monder DS, Karan K. An Effective Property Model for Infiltrated Electrodes in Solid Oxide Fuel Cells. Journal of the Electrochemical Society. 2014;161:F83-F93.

[2] Deng X, Petric A. Geometrical modeling of the triple-phase-boundary in solid oxide fuel cells. Journal of Power Sources. 2005;140:297-303.

[3] Costamagna P, Costa P, Antonucci V. Micro-modelling of solid oxide fuel cell electrodes. Electrochimica Acta. 1998;43:375-94.

[4] Janardhanan VM, Heuveline V, Deutschmann O. Three-phase boundary length in solid-oxide fuel cells: A mathematical model. Journal of Power Sources. 2008;178:368-72.

[5] Bouvard D, Lange FF. Relation between percolation and particle coordination in binary powder mixtures. Acta Metallurgica et Materialia. 1991;39:3083-90.

[6] Chen D, Lin Z, Zhu H, Kee RJ. Percolation theory to predict effective properties of solid oxide fuel-cell composite electrodes. Journal of Power Sources. 2009;191:240-52.

[7] Suzuki M, Oshima T. Estimation of the Co-ordination Number in a Multi-Component Mixture of Spheres. Powder Technology. 1983;35:159-66.

[8] Zhang Y, Sun Q, Xia C, Ni M. Geometric Properties of Nanostructured Solid Oxide Fuel Cell Electrodes. Journal of the Electrochemical Society. 2013;160:F278-F89.
[9] Synodis MJ, Porter CL, Vo NM, Reszka AJL, Gross MD, Snyder RC. A Model to Predict Percolation Threshold and Effective Conductivity of Infiltrated Electrodes for Solid Oxide Fuel Cells. Journal of the Electrochemical Society. 2013;160:F1216-F24.
[10] Bertei A, Pharoah JG, Gawel DAW, Nicolella C. A Particle-Based Model for Effective Properties in Infiltrated Solid Oxide Fuel Cell Electrodes. Journal of the Electrochemical Society. 2014;161:F1243-F53.
[11] Zhu W, Ding D, Xia C. Enhancement in Three-Phase Boundary of SOFC Electrodes by an Ion Impregnation Method: A Modeling Comparison. Electrochemical and Solid-State Letters. 2008;11:B83.
[12] Hardjo E, Monder D, Karan K. Numerical Modeling of Nickel-impregnated Porous YSZ-supported Anodes and Comparison to Conventional Composite Ni-YSZ Electrodes. ECS Transactions. 2011;35:1823-32.
[13] Chen M, Song C, Lin Z. Property models and theoretical analysis of novel solid oxide fuel cell with triplet nano-composite electrode. International Journal of Hydrogen Energy. 2014;39:13763-9.
[14] Jiang SP. Nanoscale and nano-structured electrodes of solid oxide fuel cells by infiltration: Advances and challenges. International Journal of Hydrogen Energy. 2012;37:449-70.
[15] Bertei A, Nicolella C. A comparative study and an extended theory of percolation for random packings of rigid spheres. Powder Technology. 2011;213:100-8.
[16] Reszka AJL, Snyder RC, Gross MD. Insights into the Design of SOFC Infiltrated Electrodes with Optimized Active TPB Density via Mechanistic Modeling. Journal of the Electrochemical Society. 2014;161:F1176-F83.
[17] Zhang Y, Xia C. A particle-layer model for solid-oxide-full-cell cathodes with different structures. Journal of Power Sources. 2010;195:4206-12.
[18] Kishimoto M, Lomberg M, Ruiz-Trejo E, Brandon NP. Enhanced triple-phase boundary density in infiltrated electrodes for solid oxide fuel cells demonstrated by high-resolution tomography. Journal of Power Sources. 2014;266:291-5.

Figure

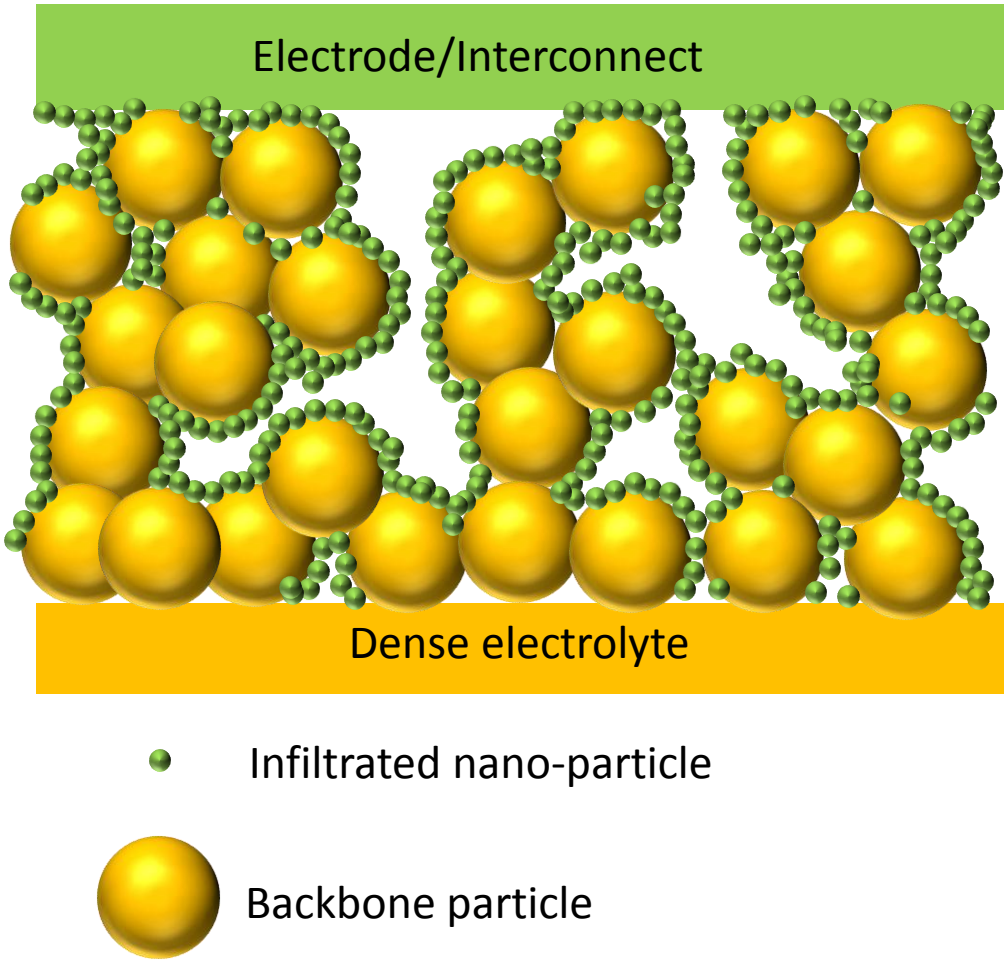
Electrode/Interconnect
Dense electrolyte
Infiltrated nano-particle
Backbone particle